We are IntechOpen, the world's leading publisher of Open Access books Built by scientists, for scientists

4,800
Open access books available

122,000
International authors and editors

135M
Downloads

Our authors are among the

154
Countries delivered to

TOP 1%
most cited scientists

12.2%
Contributors from top 500 universities

CLARIVATE ANALYTICS BOOK CITATION INDEX INDEXED

WEB OF SCIENCE™

Selection of our books indexed in the Book Citation Index in Web of Science™ Core Collection (BKCI)

Interested in publishing with us?
Contact book.department@intechopen.com

Numbers displayed above are based on latest data collected.
For more information visit www.intechopen.com

3

The Group Velocity Picture of Metamaterial Systems

Xunya Jiang, Zheng Liu, Wei Li, Zixian Liang, Penjun Yao, Xulin Lin, Xiaogang Zhang, Yongliang Zhang and Lina Shi
State Key Laboratory of Functional Materials for Informatics, Shanghai Institute of Microsystem and Information Technology, CAS, Shanghai
China

1. Introduction

Metamaterial is a very fresh concept in modern photonics, which are referred to a new class of electromagnetic media whose permittivity or permeability is beyond traditional values. Fifty years ago, a kind of new materials whose permittivity ϵ and permeability μ are simultaneously negative was theoretically predicted to possess a negative refractive index n with many unusual properties[1]. In last decade, negative-n metallic resonating composites and two dimensional (2D) isotropic negative-n material have been constructed[2, 3], and negative light refraction was observed[4]. The unconventional properties of such materials, such as the evanescent wave could be amplified by negative-n so that the sub-wavelength resolution could be achieved[5], have drawn an increasing amount of attention in both science and engineering[6]. After negative-n material, more such unconventional materials are found, so that a new concept "metamaterial" is generated, which termed for the effective medium with very special permittivity ϵ_{eff}, or permeability ϵ_{eff}, or both, over a certain finite frequency band. Such physical media are composed of distinct elements (photonic atoms) which are generally made of sub-wavelength metallic structure and their size scale is much smaller than the wavelengths in the frequency range of interest. Thus, the effective composite media could be considered homogeneous at the wavelengths under consideration. Since their abnormal properties and related totally new phenomena can even go beyond the traditional physical limit, metamaterial becomes one of hottest topics in modern photonics.

However, from the beginning of the metamaterial research, there are many arguments for a lot topics, such as, Pendry's famous pioneer work of superlens[5] was commended several times. One main reason of so many arguments is that the light *beams* in different metamaterials seem to be too strange (even weird) to be acceptable. So it is natural to argue whether these beams could be real. Another main reason is a general weakness of current metamaterial studies which mainly focus on the single frequency properties and neglect the dispersion. Actually these two reasons are related. We know that the dispersion , in the frame of classical electrodynamic, means the electromagnetic response of the material to the external field, and plays the key role in the metamaterial abnormal properties. For these strange beams, such as negative refraction beams, with dispersion we can obtain the group velocity (energy velocity) which determine the beams propagating direction. So the group velocity should be the basic picture for us to understand these strange beams and help us to design related devices. More

seriously, the dispersion is related with some very basic limitations of this world, *e.g*. the causality limitation that the group velocity in metamaterial should be less than the vacuum light speed. If our design of devices is based on the metamaterials which violate these basic limitations, the design surely can not work since such metamaterial could not exist in this world. From this view, the group velocity picture is not only needed in understanding and explanation, but also required in research of some topics and design of devices. For instance, in the research of the limitation of the cloak[7, 8] and abnormal phenomena on the interface of the hyperbolic metamaterial[9], if we neglect the dispersion of material, from group velocity picture we will immediately find that we have fallen into a superluminal trap, since the energy velocity in such artificial systems is divergent. So, the group velocity picture can help us avoid such traps.

As a basic value for revealing the complex propagating process, abnormal group velocity has been studied for decades. In the early 1960's the group velocity in material has been studied by Brillouin[10] and the group velocity in strongly scattering media is investigated by J. H. Page, Ping Sheng *et al.* in 1996[11], which indicate that the physical origin of the remarkably low velocities of propagation lies in the renormalization of the effective medium by strong resonant scattering. So far, metamaterials generally are composite of "photonic atoms" which can scatter light coherently. And all abnormal properties of metamaterials, *e.g.* these strange beams, are from these complex coherent scattering. Another byproduct of these scattering is the (abnormal) group velocity. In other words, the strange beam and the abnormal group velocity are two sides of a same coin. Further more, with some abnormal group velocity, such as the extremely slow light, we can design new signal-processing devices or new detecting devices. Hence, exploring the group velocity in metamaterial is very vital for revealing mechanism and the design of the real optical devices.

The numerical simulation takes an important role in research for modern photonics. For metamaterial, since the difficulties of experimental realization, the numerical tools become very essential for researchers. But, in some frequency domain simulation softwares, the dispersion is neglected totally. As we discussed above, we think such softwares can misleading researchers to some imaginary metamaterial which can not exist in this world. Such as for cloaking study, these softwares could present perfect invisibility very easily, but from our study[7, 8], that is misleading one. We strongly recommend the time-domain softwares, such as finite-difference time-domain (FDTD) method or finite-element time-domain(FETD) method. Their simulating results are much more convincible since they are generally with physical dispersion in the simulation and fit for metamaterial studies.

This paper is organized as following. The first section is the introduction in which we generally introduce the group velocity picture of the metamaterial study. As we have discussed, the group velocity is the key for understanding these abnormal properties of metamaterials and also can help us to avoid some traps of basic physical limit. We have also commended the softwares fit for metamaterial studies.

In the second section, the optical properties of the interface between hyperbolic meta-material (with anisotropic hyperbolic dispersion) and common dielectric is investigated. With material dispersion, a comprehensive theory is constructed, and the hyperlens effect that the evanescent wave can be converted into the radiative wave is confirmed. At the inverse process of hyperlens, we find a novel mechanism to compress and stop (slow) light at wide frequency

range, which can be used as a removable memory or a light trap. All theoretical results are demonstrated by finite-difference time-domain simulation.

In the third section we propose general evanescent-mode-sensing methods to probe the quantum electrodynamics (QED) vacuum polarization. The methods are based on the phase change and the energy time delay of evanescent wave caused by small dissipation. From our methods, high sensitivity can be achieved even though the external field, realizable in contemporary experiments, is much smaller than the Schwinger critical field.

In the forth section the image field of the negative-index superlens with the quasi-monochromatic random source is discussed, and dramatic temporal-coherence gain of the image in the numerical simulation is observed, even if there is almost no reflection and no frequency filtering effects. From the new physical picture, a theory is constructed to obtain the image field and demonstrate that the temporal coherence gain is from different "group" retarded time of different optical paths. Our theory agrees excellently with the numerical simulation and strict Green's function method. These study should have important consequences in the coherence studies in the related systems and the design of novel devices.

In the fifth section, the dynamical processes of dispersive cloak by finite-difference time-domain numerical simulation are carried out. It is found that there is a strong scattering process before achieving the stable state and its time length can be tuned by the dispersive strength. Poynting-vector directions show that the stable cloaking state is constructed locally while an intensity front sweeps through the cloak. Deeper studies demonstrate that the group velocity tangent component $V_{g\theta}$ is the dominant factor in the process. This study is helpful not only for clear physical pictures but also for designing better cloaks to defend passive radars.

In the sixth section, the limitation of the electromagnetic cloak with dispersive material is investigated based on causality. The results show that perfect invisibility can not be achieved because of the dilemma that either the group velocity V_g diverges or a strong absorption is imposed on the cloaking material. It is an intrinsic conflict which originates from the demand of causality. However, the total cross section can really be reduced through the approach of coordinate transformation. A simulation of finite-difference time-domain method is performed to validate the analysis.

In the last section, we give a summary of our works.

2. Hyper-interface, the bridge between radiative wave and evanescent wave

Many new phenomena are observed at the interfaces between meta-material and common dielectric material, such as the negative refraction which is found at the left-handed material(LHM) surface More interestingly, the evanescent wave (EW) could be amplified at LHM interface so that the super-resolution could be achieved[14]. Besides the LHM, there is another class of anisotropic metamaterial, so called "hyperbolic medium"(HM), in which one of the diagonal permittivity tensor components is negative and results in a hyperbolic dispersion. For convenience, we call the interface between a HM and a common dielectric material as "hyper-interface"(HI). Some surprising electromagnetic properties of HI are intensively studied recently[15, 16]. For instance, HI can convert the EW into the radiative wave (RW) so that the sub-wavelength information could be observed at far-field, which is called "hyper-lens" effect[15]. Very recently it is found that when HI is perpendicular to one

asymptote of HM dispersion, abnormal omnidirectional transmission occurs[17]. Although some theoretical and experimental works [16] have demonstrated that the EW really can be converted into RW by HI of the layered cylindrical HM, a full theory involving the “material dispersion"(will be explained later) has not been given so far. For meta-material systems, if without physical dispersion, some abnormal optical properties can not be clearly explained and the dynamical study of wave propagation can not be carried out[20]. Even more seriously, the causality violation because of the superluminal group velocity ($v_g > c$) in HM is pointed out[18], which makes the observed hyper-lens effect doubtful. To solve these problems and predict new phenomena, more robust theory with stronger base is needed.

On the other hand, to compress and to stop (slow) light pulses are very essential for modern optical/photonics research and signal processing. Hence, a new mechanism, which can compress and stop (slow) light pulses and is frequency and direction insensitive, would induce wide interest in related directions.

In this Letter, we theoretically and numerically investigate the novel optical properties of flat HI[22], in which, unlike the cylindrical HI, the translational symmetry guarantees the simple physical picture for intuitive understanding, the quantitative study of the conversion between EW and RW *etc*.

A general theory of HI is constructed with physical dispersion of HM. On the HI, not only the conversion from EW to RW (CER) of hyperlens is confirmed, when RW is incident from HM to dielectric(the inverse process of hyper-lens), but also the almost total conversion from RW to EW (CRE) can occur, *i.e*. there is "no-transmission and no-refelection" (NTNR). More important we find that this is a new mechanism to compress and stop (slow) light pulses in wide frequency and direction range with many potential applications. Theoretically and numerically we demonstrate that the superluminal group velocity in hyperlens is artificial since the HM material dispersion is neglected in previous study[18]. At last, the feasibility to realize these functions on real structures is discussed. All theoretical results are demonstrated by finite-difference-time-domain (FDTD) simulations.

Our model is as follows. Assuming two plane waves are incident to HI from HM and isotropic dielectric, and scattered from HI, as shown in the upper-right insert of Fig.(1). The HI is in the x-z plane, while the incident surface and both HM optical axes lie in the x-y plane. The incident waves are chosen as TM wave with field components (E_x, E_y, H_z) and same “parallel wave-vector" k_x. The HM is with the permittivity tensor as

$$\hat{\epsilon}_p = \begin{pmatrix} \epsilon_1(\omega) & 0 \\ 0 & \epsilon_2 \end{pmatrix} \tag{1}$$

in its principle axes coordinate, where $\epsilon_1 < 0$ and $\epsilon_2 > 0$ are assumed. And the permittivity of isotropic dielectric material is ϵ. The essential point of our model is that the negative diagonal component is dispersive $\epsilon_1 = \epsilon_1(\omega)$, which is called *material dispersion* in our study. It is well known that dispersion is physically required for real meta-materials with abnormal effective constitutive coefficients, such as negative permittivity. We will see that the material dispersion will help us to obtain self-consistent explanation of abnormal optical properties of HI and to avoid causality violation.

For simplicity, the HM is nonmagnetic and Gaussian unit is employed throughout the paper. We define the angle between the HI (or x axis) and the positive-ϵ principle axis of HM is θ,

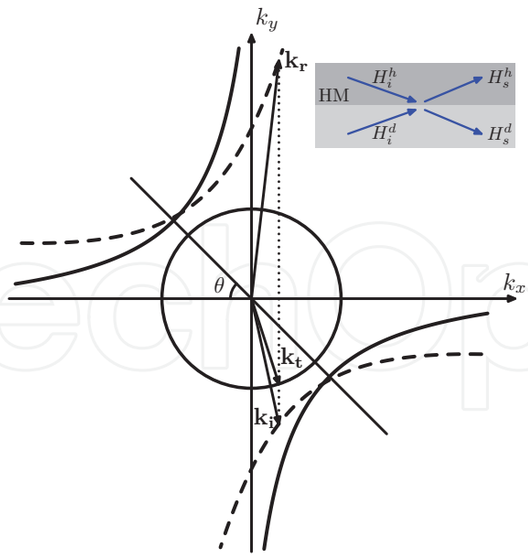

Fig. 1. The frequency contour of HM and isotropic dielectric material in k space. The inset: the schematic figure of our model.

then the most general frequency contour in k space of HM is:

$$\frac{(k_x\cos\theta - k_y\sin\theta)^2}{\epsilon_2} - \frac{(k_y\cos\theta + k_x\sin\theta)^2}{|\epsilon_1|} = (\frac{\omega}{c})^2 \tag{2}$$

In the HM region and the isotropic dielectric region the fields can be expressed uniformly as $\mathbf{H}^\sigma = \mathbf{e_z}(H_{iz}^\sigma + H_{sz}^\sigma)e^{ik_x x - i\omega t}$, $\mathbf{E^{\text{œ}}} = [\mathbf{e_x}(c_{ix}^\sigma H_{iz}^\sigma + c_{sx}^\sigma H_{sz}^\sigma) + \mathbf{e_y}(c_{iy}^\sigma H_{iz}^\sigma + c_{sy}^\sigma H_{sz}^\sigma)]e^{ik_x x - i\omega t}$ where the coefficients are defined as $c_{\nu\xi}^\sigma = E_{\nu\xi}^\sigma / H_{\nu z}^\sigma$ with $\nu = i, s$ for the incident fields to HI or the scattered fields from HI; $\xi = x, y$; $\sigma = h, d$ for the HM region or dielectric region. Since the translation symmetry of flat HI, the wave-vector parallel component k_x is continuous at both regions. In following discussion, the k vectors are normalized by $\tilde{k}_{\nu\xi}^\sigma = k_{\nu\xi}^\sigma / k_0$ where $k_0 = \omega/c$.

To explore the transmission and reflection properties of HI, we define a scattering matrix associated with the incident fields and out-going fields at HI.

$$(H_{sz}^h, H_{sz}^d)^T = S_{2\times 2}\,(H_{iz}^h, H_{iz}^d)^T \tag{3}$$

where the superscript T means the matrix transpose, $S_{11} = -(c_{ix}^h\epsilon + \tilde{k}_y^d)/(c_{sx}^h\epsilon + \tilde{k}_y^d)$, $S_{12} = (-c_{ix}^h\epsilon + \tilde{k}_{iy}^d)/(c_{sx}^h\epsilon - \tilde{k}_{iy}^d)$, $S_{21} = (c_{sx}^h - c_{ix}^h)\epsilon/(c_{sx}^h\epsilon + \tilde{k}_y^d)$, and $S_{22} = -2\tilde{k}_{iy}^d/(c_{sx}^h\epsilon - \tilde{k}_{iy}^d)$. From the standard boundary conditions, the coefficients $c_{i(s)x}^h$, $c_{i(s)x}^d$ are worked out to be $c_{i(s)x}^h = (-\tilde{k}_{i(s)y}^h\alpha^2 + \tilde{k}_x\alpha\gamma)/(|\epsilon_1|\epsilon_2)$; $c_{i(s)x}^d = -\tilde{k}_{i(s)y}^d/\epsilon$, where factors α, γ are defined as $\alpha = (\epsilon_1\sin^2\theta - \epsilon_2\cos^2\theta)^{\frac{1}{2}}$; $\gamma = (|\epsilon_1| + \epsilon_2)\sin 2\theta/2\alpha$, and the values of $\tilde{k}_{i(s)y}^d = \pm\sqrt{\epsilon - \tilde{k}_x^2}$ and $\tilde{k}_{i(s)y}^h$ and $\tilde{k}_{i(s)y}^h = (\pm(|\epsilon_1|\epsilon_2(\tilde{k}_x^2 + \alpha^2))^{1/2} + \tilde{k}_x\alpha\gamma)/\alpha^2$ are uniquely determined by Eq.(2), respectively. From Eq.(3) we can easily get the reflection and transmission coefficients across the HI from upper to down, or inverse. For the case of hyperlens that the wave is incident

from the isotropic medium to the HM, $t_{dh} = S_{22}$; $r_{dh} = S_{12}$. When $\tilde{k}_x^2 > \epsilon$, the incident and the reflected waves in the isotropic dielectric are EWs with y-component wave-vectors as $\tilde{k}_{iy}^d = i\sqrt{\tilde{k}_x^2 - \epsilon} = -\tilde{k}_{sy}^d \equiv i\kappa$. We note that, although single EW can not carry net energy current(time averaged), two EWs, *i.e.* the incident and reflected EWs, *can* carry net energy current $\vec{S}_{iy}$ in isotropic dielectric medium, since the reflected EW gains an extra-phase from complex reflecting coefficient r_{dh}. The energy current $\vec{S}_{iy}$ carried by two EWs can be converted by HI into the RW energy current $\vec{S}_{ty}$ in the HM:

$$\begin{aligned} |\vec{S}_{iy}| &= \frac{\kappa}{\epsilon}\mathrm{Im}(r_{dh}) = -\frac{2c_{sx}^h\kappa^2}{c_{sx}^{h\,2} + \kappa^2} \\ &= |\vec{S}_{ty}| = -\frac{1}{2}|t|^2 c_{tx} \end{aligned} \tag{4}$$

From Eq(4), the hyper-lens effect and the image-improving by CER could be quantitatively studied.

After confirming CER on HI, it is natural to wonder if CRE can occur too, or if there are other novel phenomena on HI. Next we will study the inverse process of hyper-lens, *i.e.* the RW is incident from HM and the transmitted field is in the dielectric. For such inverse processes, there is a critical condition $\theta = \theta_c \equiv \arctan\sqrt{\epsilon_2/|\epsilon_1|}$, which means HI ($x$ axis) perpendicular to one of hyperbola-dispersion asymptotes, or in other words, the asymptote is parallel with y axis now, as shown by the the solid lines in Fig.(1). At this critical condition, especially when the transmitted wave is EW, we will find CRE with NTNR, compressing and stopping light pulses, etc.

Before we get into detailed derivation, for the critical case ($\theta = \theta_c$) we first present two seemingly conflicting conclusions of *reflected wave* from two different arguments, which will clearly show the most tricky point of HI.

The first argument is from the “intuitive way" which is based on Fig.(1). Since there is no reflection wave-vector on the dispersion curve to satisfy the k_x continuity, we intuitively expect that there should be *no* reflected wave with omnidirectional incidence. If the incident angle is large enough $\tilde{k}_x^2 > \epsilon$ so that the transmitted field is EW, and since a single EW can not carry energy current, NTNR is the only possible choice and we expect that CRE will occur on HI. But from the second argument based on Eq.(4), we will obtain a different result. Since $\theta = \theta_c$ is a critical case, we should be more careful and discuss in a more subtle and strict way.

We first suppose the $\theta \neq \theta_c$ as shown by dashed lines Fig.(1), so the finite $\tilde{k}_{ry}$ of reflected field for a fixed $\tilde{k}_x$ can be found. Next we let the angle θ to approach θ_c continuously (which can be realized physically by choosing different direction of HI), then we find that $\tilde{k}_{ry} \to \infty$ when $\theta \to \theta_\mathrm{c}$ for a fixed $\tilde{k}_x$.

But surprisingly, when $\theta \to \theta_\mathrm{c}$, the reflection coefficient r_{hd}, calculated from Eq.(4) as $\lim_{\theta\to\theta_c} r_{hd} = (\epsilon\tilde{k}_x - \sqrt{|\epsilon_1|\epsilon_2(\epsilon - \tilde{k}_x^2)})/(\epsilon\tilde{k}_x + \sqrt{|\epsilon_1|\epsilon_2(\epsilon - \tilde{k}_x^2)})$ is not zero, and the reflected energy current is not zero too. So the theoretical result seems against our intuition.

To explain the conflicting results, we need to calculate the group velocity inside HM with material dispersion, which will also show that the superluminal group velocity is artificial.

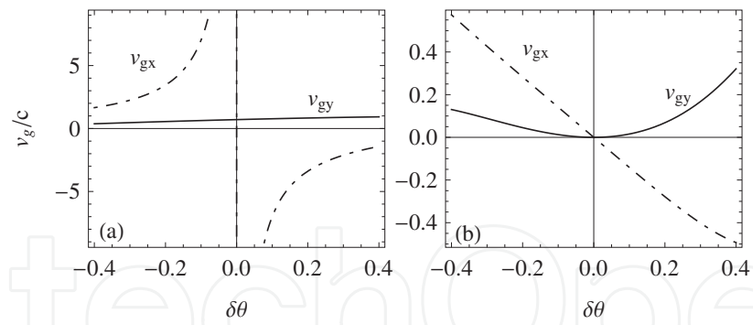

Fig. 2. Two components of $\vec{v}_g$ of reflected field in HM. (a)Without material dispersion of ϵ_1, (b)with material dispersion.

The most general expression of the group velocity of the reflected wave (which is also the group velocity of transmitted field in HM of hyperlens case) can be obtained from Eq.(2) as:

$$v_{gx} = \frac{2c\epsilon_1\epsilon_2(\alpha\gamma\tilde{k}_y^h + \tilde{k}_x\beta^2)}{\epsilon_2^2\epsilon_1(\omega)'\omega\tilde{k}_y^{p2} - \epsilon_1^2\epsilon_2(\omega)'\omega\tilde{k}_x^{p2} - 2\epsilon_1^2\epsilon_2^2} \tag{5a}$$

$$v_{gy} = \frac{2c\epsilon_1\epsilon_2(\alpha\gamma\tilde{k}_x - \tilde{k}_y^h\alpha^2)}{\epsilon_2^2\epsilon_1(\omega)'\omega\tilde{k}_y^{p2} - \epsilon_1^2\epsilon_2(\omega)'\omega\tilde{k}_x^{p2} - 2\epsilon_1^2\epsilon_2^2} \tag{5b}$$

where $\tilde{k}_x^p = (\tilde{k}_x\cos\theta - \tilde{k}_y^h\sin\theta)$ and $\tilde{k}_y^p = (\tilde{k}_y^h\cos\theta + \tilde{k}_x\sin\theta)$ are the "k components" in the principal-axes coordinate of HM and $\beta = (\epsilon_2\sin^2\theta - \epsilon_1\cos^2\theta)^{\frac{1}{2}}$. From Eq.(5), we find that, if the material dispersion of HM is neglected $\partial\epsilon_1/\partial\omega = \partial\epsilon_2/\partial\omega = 0$, then we will obtain the superluminal group velocity as shown in Fig.2(a). When $\theta \to \theta_c$, the v_g even diverges.

But with material dispersion, the x and y components of v_g is recalculated, and we find that there is no $v_g > c$ at all cases, as shown in Fig.2(b) in which two components of v_g versus $\theta - \theta_c$ based on Eq.(5), with the parameters $\epsilon_2' = 0$, $\epsilon_2 = 1$, $\epsilon_1(\omega) = (1 - \frac{\omega_p^2}{\omega^2})$[21] and $\omega = \omega_p/\sqrt{2}$, $\theta_c = \pi/4$. When approaching the critical angle $\theta \to \theta_c$, two components can be approximated as:

$$\lim_{\theta\to\theta_c} v_{gx} \sim \frac{1}{\epsilon_1'(\omega)}(k_{ry}^h)^{-1} \tag{6a}$$

$$\lim_{\theta\to\theta_c} v_{gy} \sim \frac{k_x}{\epsilon_1'(\omega)}(k_{ry}^h)^{-2} \tag{6b}$$

. Since $\tilde{k}_{ry}^h \to \infty$ at the critical angle θ_c, the group velocity of the reflected wave should be zero $\mathbf{v}_g = 0$ at the critical angle, as shown in Fig.2(b) too.

What does the zero-group velocity of reflected wave mean? The analysis will give us clear answer. As we have pointed out,since the reflected energy current $\vec{S}_r$ is not zero and $\vec{S}_r = v_g W$ where W is the energy density of reflected wave, hence the energy density W must be infinite large at the critical angle. From Eq.(2), we can obtain that the electric field of reflected wave $|\mathbf{E_r^h}|$ is really divergent at the critical angle. The divergent field strength means that it need *infinite long time* to accumulate energy at HI for the reflected field. In other words, there is no reflected wave physically, as our intuition has told us. When the incident angle is large enough

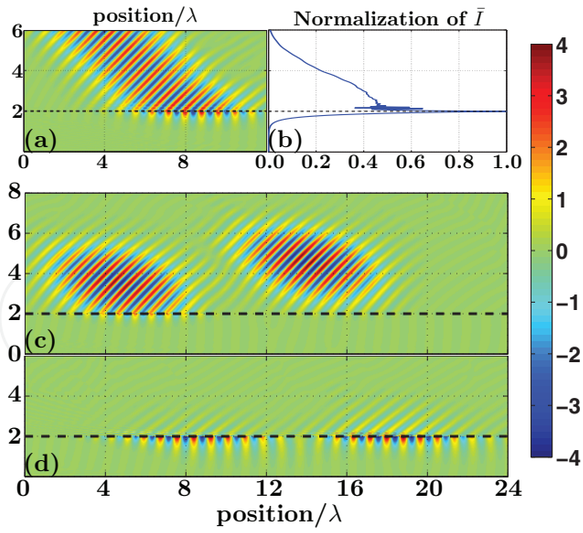

Fig. 3. (a)The magnetic field H_z distributions for a Gaussian beam incident on the interface with $|\tilde{k}_x| > \sqrt{\epsilon}$. (b)The averaged field intensity versus the vertical distance to the HI. (c)Two pulses are arriving at HI at different time. (d) The fields of two pulses, which stay at the incident positions, at 14 periods after the pulse arriving.

$\tilde{k}_x^2 > \epsilon$, since the energy of incident RW can not be transmitted, also can not be reflected, the only answer is that the energy is stored at the HI or CRE occurs. Thus, we can have a self-consistent explanation for our seemingly conflicting results.

To confirm our theoretical discussion at θ_c, the FDTD simulation [79] with strict physical HM dispersion (Drude mode) which satisfies Kramar-Kronig relation, is done. The parameter of HM and dielectric are $\epsilon_1 = -3,\ \epsilon_2 = 3$, and $\epsilon_l = 1.1$. For the case($\tilde{k}_x > \epsilon$), as shown Fig.3(a), a light beam is incident from HM to HI in 45^0 angle,as we predicted, there is no reflection and no transmission, and the field energy is accumulated at HI and stopped there. More detailed observation shows that at the boundary the field energy is mainly at the dielectric side, as shown Fig.3(b).

We also has checked the group velocities of hyperlens cases and and find no violation of the causality. Actually, in FDTD simulation, if there is superluminal group velocity the program will be numerically unstable.

The dynamical study, such as with the pulse incidence, can reveal more interesting phenomena of HI. Since the group velocity along HI is zero at NTNR case as discussed, we expect that the pulse energy will accumulate on HI and stay at the incident position until it is dissipated because of absorption of HM.

The numerical experiments with incident pulses by FDTD are also done. As shown in Fig.3(c) and (d), two pulses arrive at the HI at different time, then they stop at the incident positions on HI. The pulse vertical length is compressed to almost zero, but their width keeps same so that they are still well separated in Fig.3(d). We emphasize at here that this is a novel mechanism to compress and stop (slow) light pulses with special advantages. The first advantage is that this mechanism works at very wide frequency and wide incident-angle range, which is confirmed by FDTD simulation in Fig.3 with incident of pretty short pulses. The frequency and incident-angle insensitivity is because the mechanism is from a simple geometry property,

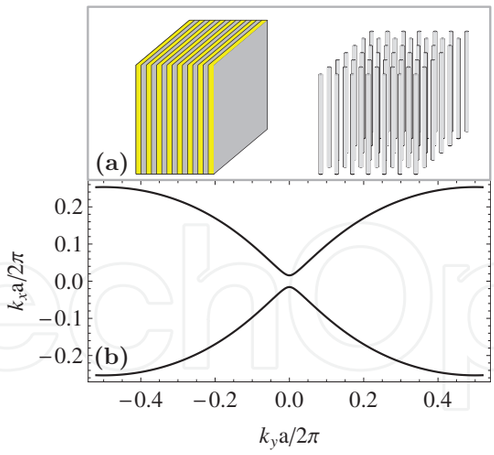

Fig. 4. (a) The structures of real HM: the periodic metal-dielectric layers and the periodic metal nano-wires embedded in a dielectric matrix. (b) The frequency contour of periodic metal-dielectric layers.

i.e. the HI (x axis) perpendicular to one of hyperbola-dispersion asymptotes. The second is that the decay (because of dissipation) of trapped field on HI is much slower than in common metallic material since the trapped field energy is mainly in the dielectric side as shown in Fig.3(b). The third is that the trapped signals are easy to take out (read) since they are on the interface. Because of these advantages, HI could be used as a removable recorder (dynamical memory) in optical/photonic signal processing, or as a wide-frequency wide-angle light trapper in photovoltaic devices.

However, we should point out that the above theoretical and numerical studies are with the assumption of the ideal hyper-dispersion, which is still void when $k_{ry} \to \infty$. In reality, such HM does't exist, so that we need to study the limit of hyper-dispersion of realizable HM. HM can be realized by many structures, i.e. one-dimensional (1D) periodic metal-dielectric binary layers [24, 25] or two-dimensional (2D) periodic metallic lines[26], as shown in Fig.4(a). For these structures, the dispersion relation can be calculated exactly. In Fig.4, the calculated frequency contour of a 1D metal-dielectric binary layers is shown, from which we can see that the effective HM medium is not available anymore when $|k|$ approaches π/a. Based on this limit, we can roughly estimate the slow limit of group velocity by $v_{gx} \sim \frac{1}{\epsilon_1'(\omega)}(k_{ry}^h)^{-1} \propto 1/\gamma_s$ and $v_{gy} \sim \frac{k_x}{\epsilon_1'(\omega)}(k_{ry}^h)^{-2} \propto 1/{\gamma_s}^2$, where $\gamma_s = k_{ry}/k_0$ is the slowing coefficient. For the 2D metallic-line structure, from the modern technical limit we assume the smallest lattice constant as $a = 10$nm. If the incident is the micro-wave $\omega = 5.8$GHz ($\gamma_s \sim 10^7$) and $\epsilon_1'(\omega) = 6.9 \times 10^{-10}$s as in Ref [27], we obtain $v_{gx} \sim 4.6$m/s which means considerably slow light although not totally stopped, and $v_{gy} \sim 7.07 \times 10^{-8}$m/s which means that the strongly-compressed light pulses can be easily achieved.

In conclusion, we have theoretically and numerically investigate the optical properties of HI. The theory with dispersion of meta-material is constructed and the hyperlens effect of CER is confirmed. At the inverse process of hyperlens, the abnormal phenomena of CRE with NTNR and a novel mechanism to compress and stop light in wide frequency range are revealed. Based the calculated group velocity, we demonstrate that the previously-pointed-out superluminal group velocity in HM is artificial since the material dispersion is neglected. FDTD simulations confirm that the HI has potential to be a removable optical/photonic

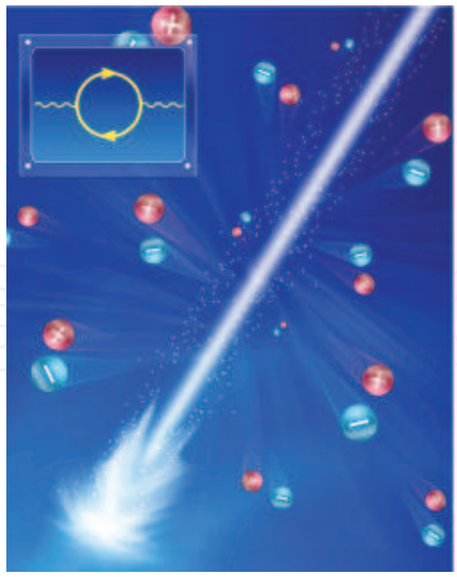

Fig. 5. The schematic picture of vacuum polarization processes with electron-positron pair generation, with which the vacuum becomes dissipative and anisotropic. The insert is the Feynman diagram of the vacuum polarization processes.

recorder, or a wide-frequency wide-angle light trapper. At last the realizability of these phenomena on the real metallic structures is discussed. Obviously, the new mechanism works not only for electromagnetic waves, but also for acoustic or matter waves if hyperbolic dispersion is available, so that more interesting phenomena and applications are waiting for further theoretical and experimental research.

3. The methods to detect vacuum polarization by evanescent modes

Vacuum is one of the most fundamental concepts in all quantum fields[30–32] since all excitations are from the vacuum and determined by vacuum in some way. Modern vacuum concept is started from quantum electrodynamics (QED), which describes the interaction between light and matter (including vacuum), and has been continually studied both experimentally and theoretically[33–38]. According to QED, the vacuum becomes weakly anisotropic, dispersive, dissipative and even nonlinear optical medium, when external electric field is approaching the Schwinger critical value $E_c \simeq 10^{18} V/m$. In other words, the real and imaginary parts of vacuum refractive index could deviate from unit and zero[34, 35], respectively. Physically, the deviation of the imaginary part is mainly from the electron-positron pair generation. However, the electron-positron pair generation, also generally called as *vacuum polarization* (VP) processes[34], which is schematically shown in Fig.1, has not been directly observed for over half century since very high E_c is beyond the contemporary technical limit. Therefore, it is natural to wonder if we can find an approach to probe VP with external field E_{ext} much smaller than E_c.

In this work, we propose evanescent-mode-sensing methods based on new mechanism to detect the QED VP, which is based on the measuring the phase change and the energy time delay of evanescent wave (EW). We find that the required external field could be one order weaker than E_c, which may be realizable by contemporary experiments.

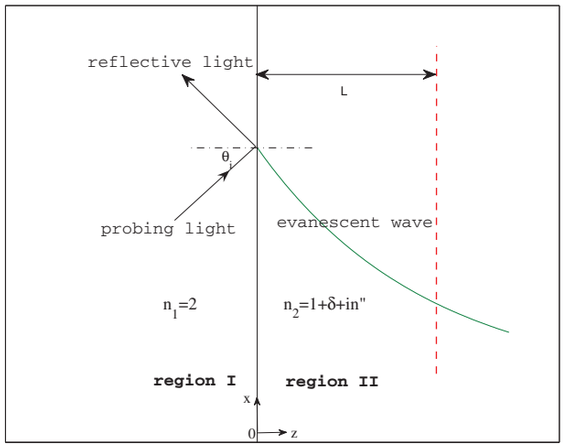

Fig. 6. The schematic diagram of our model.

The idea is from the “dual roles" of real and imaginary parts of refractive index n. Supposing a medium with complex index $n = n' + in''$, our goal is to detect the very tiny change of n' or n''. For radiative waves, since n' determines the real part of wavevector $k \simeq n'\omega/c$ and it is easy to measure the phase change or group delay, so, it is natural to choose the radiative wave to probe small change of n'. On the other hand, for radiative waves, tiny change of n'' causes an extremely small decay change which is very hard to measure in the limited lab space. However, for the evanescent waves, the roles of n' and n'' are totally exchanged, i.e., n' dominates the decay rate, while the n'' introduces a phase change which is much easier to detect. Further more, we will demonstrate that n'' can also introduce the energy propagation for EWs whose energy velocity $v_e \propto n''$ can be extremely slow. Such a slow wave can be detected by measuring the delay time τ at a short distance.

Actually, the tenneling mechanism of EW has been widely studied[39–41]. We would like to emphasize the mechanism difference between ours and that in the previous works. In Ref[41], they are based on “two interfaces" structure (a slab). Such “two-interfaces" structure will generate both evanescent modes $\exp(\pm\kappa x)$ and such two evanescent modes can carry energy current[9], which called as “tunneling mechanism". So, even if the material dissipation is neglected[41] , the energy propagation is still available. However, in our model, since there is only a single interface (Fig.2), obviously if without dissipation there will be no the energy current at all[42], then, no phase change and no the energy delay time. So, our mechanism is based on the dynamical picture and the dissipation is critical.

Here we note that, because the probing light is much weaker than the external field in our model, the nonlinear effect is negligible. For a linear system, all dynamical processes can be solved numerically by sum of multi-frequency componentsčňwhich can be obtained by Green’s function methods [42].

Our model is schematically shown in Fig.6, based on the total internal reflection (TIR) at the interface between a dielectric media n_1 (region I) and vacuum (region II). When the incident angle $\theta_i > \theta_c = arcsin(1/n_1)$, the TIR will occur and the transmitted wave in the vacuum is the EW. We choose θ_i is a little larger than θ_c to make sure that almost all frequency components

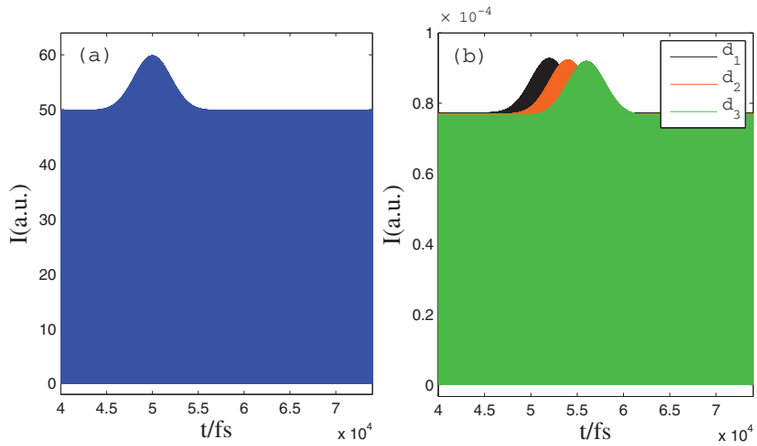

Fig. 7. The irradiance of light I versus time t, (a)the incident light at the interface; (b)the transmitted EW in region II, where the black, the red and the green lines are for the fields at the distance from the interface $d_1 = 0.1\lambda_0$, $d_2 = 0.2\lambda_0$ and $d_3 = 0.3\lambda_0$, respectively, with $\lambda_0 = 600nm$.

are totally reflected when the incidence is the slowly-varying quasi-monochromatic wave. An interferometer or a photon detector is set at distance L from the interface so that the phase and intensity change can be detected.

The time-dependent Maxwell equations are given by $\nabla \times \mathbf{E} = -\mu(z)\mu_0 \partial \mathbf{H}/\partial t$ and $\nabla \times \mathbf{H} = \epsilon(z)\epsilon_0 \partial \mathbf{E}/\partial t$, where $\epsilon(z)$ and $\mu(z)$ are the relative permittivity and the relative permeability, respectively, and $c = 1/\sqrt{\epsilon_0\mu_0}$. To obtain the concrete results, the system parameters are chosen as following, the incident angle $\theta_i = 0.1667\pi$, the refractive index of region I $n_1 = \sqrt{\epsilon_1} = 2$, and the vacuum refractive index of region II $n_2 = \sqrt{\epsilon_2\mu_2} = 1 + \delta + in''$, where $\delta << 1$ and $n'' << 1$ are the real and imaginary index deviations of vacuum, because of VP processes caused by strong external field. If the incident probing light is a plane wave, the transmitted wave in the vacuum region can be generally written in the form $E(x,z,t) = Eexp(ik_z z + ik_{\|} r_{\|} - i\omega t)$, where $k_{\|} = n_1 \sin\theta_i \omega/c$ and $k_z = \sqrt{(n_2\omega/c)^2 - k_{\|}^2}$ are the wave vectors parallel and perpendicular to the interface. For the EW, k_z is described as:

$$k_z = i\sqrt{(n_1 \sin\theta_i)^2 - (1+\delta)^2}\,\frac{\omega}{c} + \frac{n''}{\sqrt{(n_1 \sin\theta_i)^2 - (1+\delta)^2}}\,\frac{\omega}{c}. \tag{7}$$

The physical meaning of k_z is very clear that the imaginary part $Im(k_z) = \kappa_z$ corresponds to the exponential decay of the field, and the real part $Re(k_z)$ causes *a phase change because of VP*. The phase change at distance $z = L$ is

$$\Delta\phi = Re(k_z)L \propto n''L \tag{8}$$

which could be measured by interferometers[43].

Besides the phase change $\Delta\phi$, with the same model as shown in Fig.6, there is another way to detect the tiny n'' by *measuring the time delay of irradiance fluctuation [44] of the evanescent wave*. It is a dynamic process as following. First, we suppose that the incident light is not a plane wave anymore, but with a slow intensity fluctuation, as shown in Fig.7(a). Then, the question is "What will happen for the EW in region II ?" Numerically, from the strict Green's

function method with physical dissipation and dispersion, it is found that the fluctuation will propagate on the EW from the interface to far away, as shown in Fig.7(b). So, we can measure the time delay τ of the fluctuation propagation on the EW to detect the VP effect. The propagation speed of irradiance fluctuation can be obtained by the energy velocity v_e which is defined as: $v_e = |\vec{S}_z|/W$, where $\vec{S}_z = \frac{1}{2} Re\left(E \times H^*\right)|_z$ is the averaged Poynting vector along z direction, and $W \simeq \frac{1}{4}(\epsilon_0|E|^2 + \mu_0|B|^2)$ is the local energy density of the electromagnetic wave. In our model, the energy velocity is obtained as:

$$v_e = \chi \cdot n'' \tag{9}$$

with $\chi \simeq c/\left[(n_1 \sin\theta_i)^2\sqrt{(n_1 \sin\theta_i)^2 - (1+\delta)^2}\right]$, when the dissipation and dispersion are very weak. The physical meaning of v_e can be understood as the "propagation" speed of irradiance fluctuation of the EW, which can be measured[44].

Hence, experimentally the time delay τ of the irradiance fluctuation at distance L can be measured:

$$\tau = L/v_e \propto 1/n''. \tag{10}$$

Since it is *near field* phenomenon, the detecting should be very near the interface. For the VP effect, since n'' is extremely small, the "propagation" speed of the irradiance fluctuation is so slow that τ gets to peco-second level when the distance is one tenth of the wavelength $L = 60nm$.

Therefore, either the phase change $\Delta\phi$ or the time delay τ are very sensitive for n'', and the EW is a good candidate to probe the VP effect. Here, we note that the famous Kramers-Kronig relations still fit for QED vacuum[34]. Hence, the observation of imaginary part of vacuum index also confirms the dispersion of QED vacuum.

Next, we will quantitatively study the VP detect by our methods. Supposing that an external homogeneous constant electric field E_{ext}, which is perpendicular to the xz plane and smaller than the Schwinger critical electric field E_c, is applied to the vacuum (region II) only, as shown in Fig.6, then, the optical properties of the vacuum can be described by the Euler-Heisenberg Lagrangian L_{eff}[34, 37]. Physically, the imaginary part of Euler-Heisenberg Lagrangian L_{eff} is related to the imaginary part of VP operator, and therefore corresponds to the *electron-positron pair generation*.

Consequently, the vacuum refractive index can be deduced from the Lagrangian L_{eff}[34, 37, 38].

In our model, since the external magnetic field is supposed to be zero, thus the vacuum refractive index is determined only by the external homogeneous constant electric field E_{ext}. We use $n_\parallel$ and $n_\perp$ to refer the effective refractive index of vacuum when the electric field of probing light are parallel and perpendicular to the field E_{ext}, respectively. $n_\parallel$ and $n_\perp$ can be obtained from the reference [38]:$n_\parallel = 1 + \frac{2\alpha}{45\pi}y^2 + i \cdot \frac{\alpha}{4\pi}\sum_{n=1}^{\infty}\left(\frac{\pi}{y^2} + \frac{1}{n}\frac{1}{y}\right)\exp(-n\pi/y)$, and $n_\perp = 1 + \frac{7\alpha}{90\pi}y^2 + i \cdot \frac{\alpha}{4\pi}\sum_{n=1}^{\infty}\left(\frac{2}{3}\pi + \frac{1}{n}\frac{1}{y} + \frac{1}{n^2}\frac{2}{\pi}\right)\exp(-n\pi/y)$, where $y = |E_{ext}|/E_c$, and $\alpha \simeq 1/137$ is the fine-structure constant. Therefore we have $\delta = Re\left(n_{\parallel(\perp)}\right) - 1$, $n'' = Im\left(n_{\parallel(\perp)}\right)$ for $n_\parallel$ and $n_\perp$ when we solve the equations such as Eq.(7) in this letter.

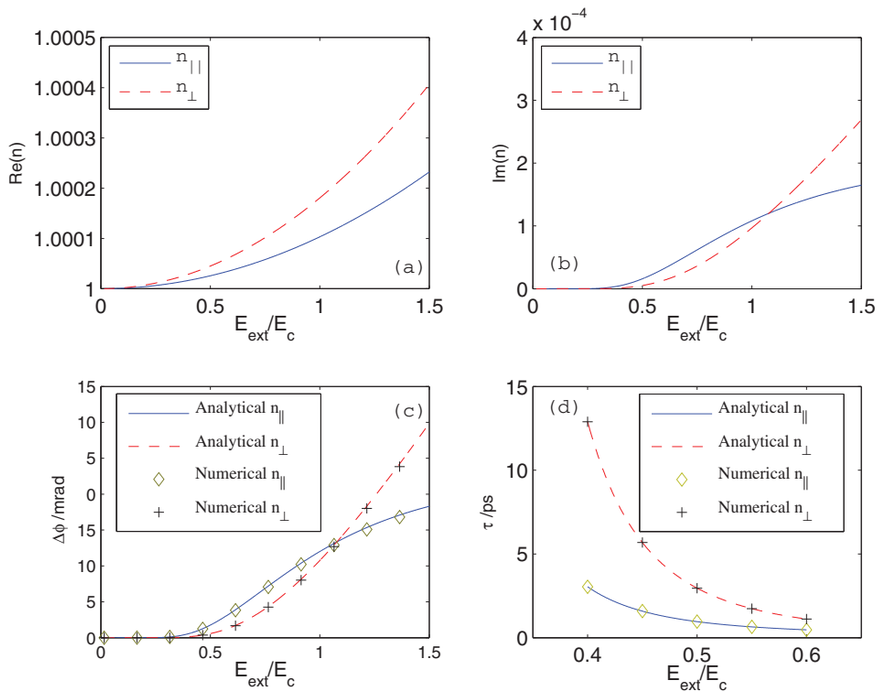

Fig. 8. (a)The real part of vacuum index $n_{\|}$ and $n_{\perp}$ versus E_{ext}; (b)The imaginary part of $n_{\|}$ and $n_{\perp}$ versus the external electric field strength; (c)$\Delta\phi$ versus with $L_p = 6\mu m$; (d)τ versus E_{ext} with $L_\tau = 60nm$. Both the results from theory and from Green's function are shown in (c) and (d).

The parameters of our model in Fig.6 are chosen as following. The wavelength of probing light is $\lambda_0 = 600nm$, the dielectric constant in the region I is $\varepsilon = 4$, and the incident angle is $\theta_{inc} = 0.1667\pi > \theta_c$, so that the field in vacuum is evanescent. The distance L for the phase detecting is $L_p = 6\mu m = 10 \times \lambda_0$, while for τ detecting is $L_\tau = 60nm = 0.1 \times \lambda_0$, respectively. The QED theoretical results of real and imaginary part of $n_{\|}$ and $n_{\perp}$ are shown in Fig.8(a) and Fig.8(b), respectively. Bring these results into Eq.(8) and Eq.(10), the phase change $\Delta\phi$ and the delayed time τ can be obtained, which are shown in Fig8(c) and Fig.8(d), respectively. Numerically, the phase change with plane wave incidence and the time delay of local amplitude maximum are calculated by Green's function method, which are also shown in Fig.8(c) and Fig.8 (d). Comparing the analytical results from Eq.(8) and Eq.(9) and numerical results, we can find that they agree with each other very well.

Next, we will analyze the possibility to observe the VP effect in experimental conditions. The recent experimental advances[45] have raised hopes that lasers may achieve fields just one or two orders of magnitude below the Schwinger critical field strength. In this case $E_{ext} \sim 0.1E_c$, from our numerical and analytical results in Fig.8, we can see the $\Delta\phi$ can get to $\sim 10^{-1}mrad$ order, which are in measuring limit of contemporary interferometer [43]. Very recently, it is supposed that the electric field E could be effectively amplified 4 times larger by coherent constructive interference of laser beams[36]. If E_{ext} can get to $0.5E_c$ by this method, not only $\Delta\phi$ can be one order larger, but also the delay time τ can get to sub peco-second level and may be measured by contemporary photon detectors.

4. The temporal coherence gain of the negative-index superlens image

Veselago predicted that the negative-index material (NIM) has some unusual properties, such as a flat slab of the NIM could function as a lens for electromagnetic (EM) waves [1]. This research direction was further pushed by works of Pendry and others [4, 5, 46–58] who showed the lens with such NIM (i.e. $\epsilon = \mu = -1 + \delta$) could be a *superlens* whose image resolution can go beyond the usual diffraction limit. After that, several beyond-limit properties of NIM systems are found, such as, the sub-wavelength cavity [59] and the waveguide [60]. Some of the theoretical results are confirmed by experiments[4, 46, 49]. And these beyond-limit properties give us new physical pictures and opportunities to design devices. Recently, new numerical [50, 51] and theoretical Green's function [52] methods are used to understand the phenomena in such systems. But so far almost all studies are done with the strictly single-frequency sources, so that the coherent properties of EM waves (or photons) in the NIM systems have not been studied to the best of our knowledge. Even more seriously, there is no theory for the propagation of coherent functions in NIM systems. The importance of coherence research can not be over-estimated since the coherence is essential in the wave interference , the imaging , the signal processing and the telecommunication [61, 62]. Can we find new frontier to go beyond at the coherent properties in NIM systems? If so, can we develop a simple theoretical method to deal with the image coherence of superlens?

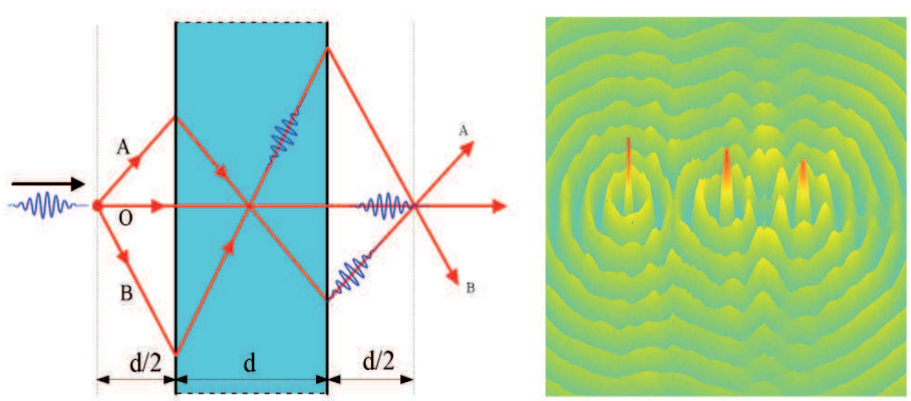

Fig. 9. The schematic diagram of our model with ray paths(left); and the typical snapshot of electric field in our FDTD simulation (right).

In this section, the finite difference time domain (FDTD) method is used in the two-dimensional (2D) numerical experiments to study the temporal coherence of the superlens image with random quasi-monochromatic sources. We observe the dramatic temporal-coherence gain of the superlens image even if the reflection and frequency-filtering effects are very weak. Based on the new physical picture of the signal (the fluctuation of random source) propagation in NIM, we construct a theory to obtain the image field and derive the equation of the temporal-coherence relation between the source and its image. The new mechanism of the temporal-coherent gain can be explained by the key idea that the signals on different paths have different "group" retarded time. Our theory excellently agrees with numerical results and the strict Green's function results.

The setup of the 2D system is shown in Fig.9. The thickness of the infinite-long NIM slab is d. To realize the negative ϵ and negative μ, the electric polarization density $\vec{P}$ and the magnetic

moment density $\vec{M}$ are phenomenologically introduced in FDTD simulation [63]. The effective permittivity and permeability of the NIM are $\epsilon_r(\omega) = \mu_r(\omega) = 1 + \omega_p^2/(\omega_a^2 - \omega^2 - i\gamma)$. In our model, $\omega_a = 1.884 \times 10^{13}/s$, $\gamma = \omega_a/100$, $\omega_P = 10 \times \omega_a$. The quasi-monochromatic field is expressed as $E(x,t) = U(x,t)exp(-i\omega_0 t)$, where $U(x,t)$ is a slowly-varying random function, $\omega_0 = \pi/20\delta_t$ is the central frequency of our random sources and $\delta_t = 1.18 \times 10^{-15}s$ is the smallest time-step in FDTD simulation. At ω_0, we have $\epsilon_r = \mu_r = -1.00 - i0.0029$. At here, we emphasize that in our FDTD simulation the smallest space-step $\delta_x = \lambda_0/20$ ($\lambda_0 = 2\pi c/\omega_0$) and the distance ($d/2 = \lambda_0$) of the source from the lens are too large to excite strong evanescent modes of NIM [50, 51, 53]. *Actually the evanescent field in our simulation can be neglected comparing with radiating field, and what we are studying is the property dominated by the radiating field.*

The random source is composed of the randomly generated plane-wave pulses, with the average pulse length t_p and the random starting phase and starting time. In the simulation, we record the field of the source and the image for a duration of $4 \times 10^5 \delta_t$ to obtain the data for analysis. For the convenience, we define $E(\omega) = \lim_{T\to\infty} \int_{-T}^{T} E(t)exp(-i\omega t)$ as the $field\ spectrum$ (FS).

Unusual phenomena.—At first, the FS width of the random source is a little too large ($\Delta\omega_s \simeq \omega_0/20$). When we observe the image temporal-coherence gain, we also find that the FS width of the image is sharper than the source ($\Delta\omega_i < \Delta\omega_s$). It is obvious that there are the frequency-filtering effects because of the NIM dispersion, such as the frequency-dependent interface reflection and focal length. After increasing the pulse-length t_p of the source, we reduce the source FS width to $\Delta\omega_s \simeq \omega_0/100$, then the reflection and focal-length difference are very small [64]. With such source, the FS widths of source and image are almost same $\Delta\omega_i \simeq \Delta\omega_s$, as shown in Fig.10a. The difference between two widths is $< 5\%$, which is our criterion of the *quasi-monochromatic* source. Even so the dramatic gain of temporal coherence is still observed. In Fig.10b, the source field (up) and the image field (down) vs time of FDTD simulation are compared. The *profiles* of them are genically similar, but the image profile is much smoother.

The normalized temporal-coherence function $g^{(1)}(\tau) =< E^*(t)E(t+\tau) > /< E^*(t)E(t) >$ (<> means the ensemble average) of the source (black) and the image (red) from FDTD simulation are shown in Fig. 11. The temporal coherence of the image field is obvious better than the source. From $g^{(1)}$, the image coherent time is obtained $T_i^{co} = \int g_i^{(1)}(\tau)d\tau = 1268\delta_t$, which is about 50% longer than the source coherent time $T_s^{co} = 860\delta_t$.

Although the gain of the spatial coherence only by propagation is well-known[62], the dramatic gain of temporal coherence is generally from the high-Q cavities, contrary to our case, which have strong filtering effects. To reveal the new mechanism of the temporal coherence gain in NIM systems, we also have done more numerical experiments in which *only* the ray near a certain incident angle (shown in Fig.9), such as only paraxial rays ($\theta \simeq 0$), can pass through the superlens. Then the image field profile vs time looks very like the source field and has no gain of coherence anymore. *Therefore, the gain of temporal coherence of the superlens image is not from one ray with certain incident angle, but probably from the interference between the rays with different incident angles.* Then, what is different between the rays with different incident angles? After carefully checking the field profiles of different-incident-angle cases, we find that the profiles have different retarded time. The larger incident angle the longer retarded time.

Physical pictures.—To deeper understand the new mechanism of coherence gain and construct our theory, we need make two physical pictures clear. The first one is about the optical path length (OPL) $\int nds$ which determines the wave phase and the refracted "paths" of rays in Fig.9 according to Fermat's principle (or Snell's law). Based on ray optics, the superlens and traditional lenses have same focusing mechanism, that all focusing rays have same OPL $\int_{paths} nds = const$ ($\int_{paths} nds = 0$ for superlens) from source to image [1]. But this picture is so well-known that it suppresses the other important picture. Because the temporal-coherence information is in the fluctuation signals of random field, the signal propagating picture should be essential for our study. *The optical signals propagate in the group velocity v_g which is always positive*. Obviously, if the path (in Fig.9) is longer (larger incident angle), the signal need a longer propagating time, which is called *group retarded time* (GRT) in this section Inside the NIM, the GRT of a path should be $\frac{d}{cos(\theta)v_g}$ (this is confirmed by our numerical experiments), where θ is the incident angle and $v_g = c/3.04$ is the group velocity of NIM around ω_0 [65]. The total GRT from source to image is $\tau_r = \tau_0/cos(\theta)$ where the $\tau_0 = d/c + d/v_g$ is the GRT of the paraxial ray. Now, the new propagating picture for a signal through superlens is that a signal, generated at at t_s from the source, will propagate on all focusing paths and arrive at

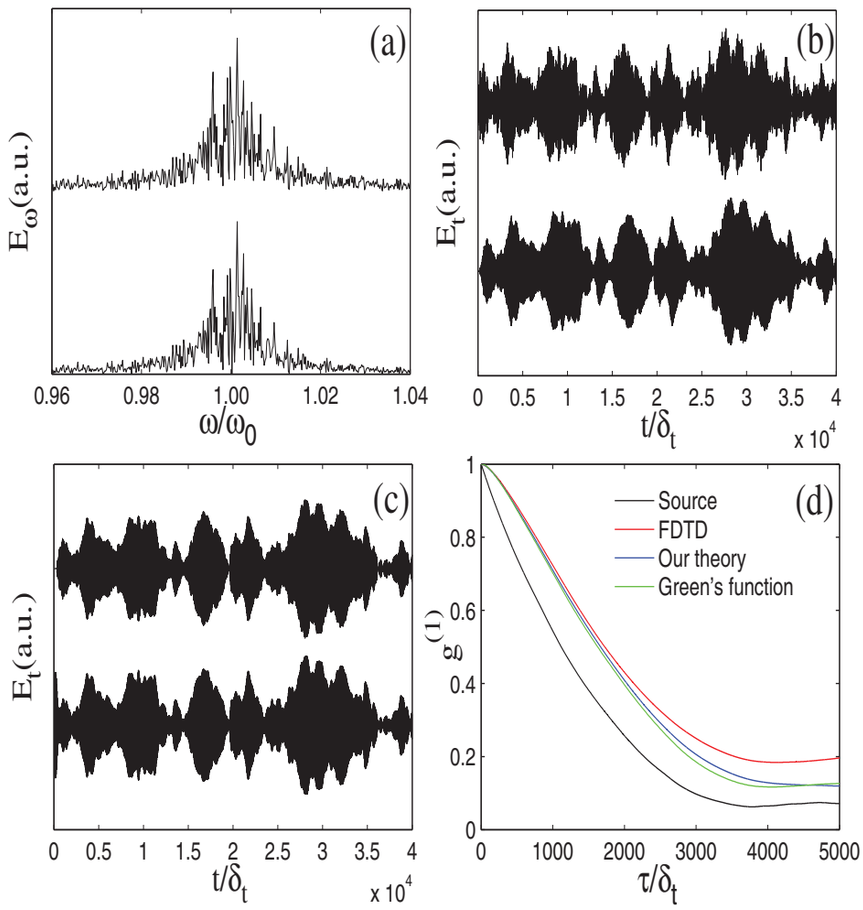

Fig. 10. (a)the FSs of the source(up) and the image(down) . (b)The electric field of the source(up) and its image (down) vs time from FDTD simulation (c) The image field vs time from Eq.(1) (up), and from the Green's function method (down).

image position at very different time $t_s + \tau_0/cos(\theta)$ from different paths(this is schematically shown in Fig.9). This picture is totally different from traditional lenses, whose images don't have obvious temporal-coherence gain because their focusing rays have same OPL *and similar GRT*.

Our theory.—Based on these analysis, we suppose that *the superlens image field of the random quasi-monochromatic source is the sum of all signals from different paths with different GRT.* This is the key point of our theory, and then the image field can be obtained:

$$E_i(t) = \frac{1}{U_0} e^{-i\omega_0 t} \sum_{paths} U_s(t - \tau_r) = \frac{1}{U_0} e^{-i\omega_0 t} \int_{-\frac{\pi}{2}}^{\frac{\pi}{2}} U_s(t - \frac{\tau_0}{\cos(\theta)}) d\theta \tag{11}$$

where $U_s(t)$ is the slowly-varying profile function of the source and U_0 is the normalization factor. In Fig.10c (up), we show the result of the image field based on Eq.(11), we can see it is in excellent agreement with the FDTD result in 2b(down). To show the interference effect of different paths, we assume there are only two paths (such as A and B in Fig.9). Based on Eq.(11) the image field is $E_i = e^{-i\omega_0 t}(U_s(t - \tau_r^A) + U_s(t - \tau_r^B))$, then the temporal coherence of image is $G(\tau) =< E_i^*(t)E_i(t+\tau) >=< U_s^*(t - \tau_r^A)U_s(t - \tau_r^A + \tau) + U_s^*(t - \tau_r^B)U_s(t - \tau_r^B + \tau) + U_s^*(t - \tau_r^A)U_s(t - \tau_r^B + \tau) + U_s^*(t - \tau_r^B)U_s(t - \tau_r^A + \tau) >$. The first two terms are same as the source field (just a time-shift) so they don't contribute to the coherence gain. The last two terms are from interference between two paths. The third (or the forth) term could be very large at the condition $\tau \simeq \tau_r^B - \tau_r^A$ (or $\tau_r^A - \tau_r^B$). This condition can always be satisfied between any two paths since τ is a continuous variable. So the interfering terms between the paths are responsible for the image temporal-coherence gain.

From Eq. (11), after the variable transformation $t_s = t - \tau_0/cos\theta$ and some algebra, the relation of the temporal coherence between the image and the source can be obtained:

$$\begin{aligned} G_i(\tau) &= < E_i^*(t)E_i(t+\tau) > \\ &= \frac{1}{U_0^2} \int_{-\infty}^{-\tau_0} dt_1 \int_{-\infty}^{-\tau_0+\tau} dt_2 h_i^*(t_1)h_i(t_2+\tau)G_s(t_2 - t_1) \end{aligned} \tag{12}$$

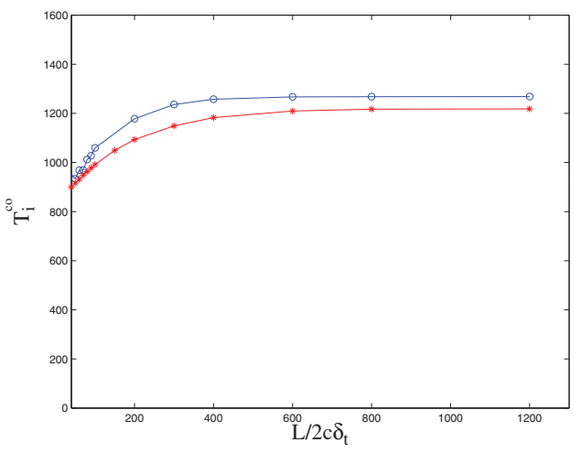

Fig. 11. The normalized temporal-coherence function $g^{(1)}$ vs time of the source field (black), and of the image field which obtained from the FDTD simulation (red), from Eq.(2) (blue) and from the Green's function method(green).

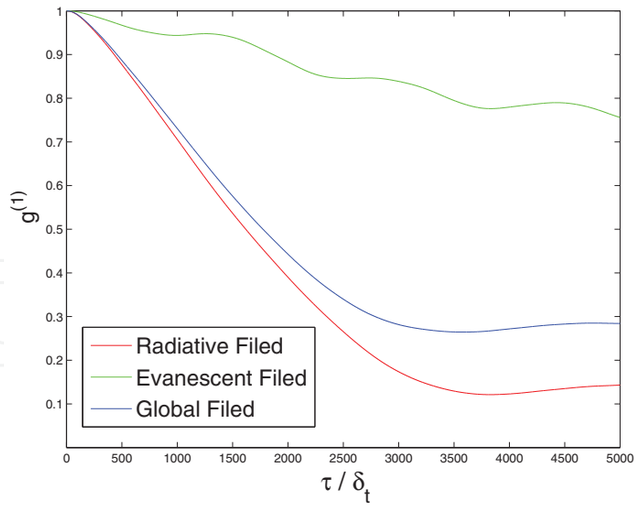

Fig. 12. The coherent time versus the superlens length L, from the FDTD simulation(blue) and from our theory (red).

where $h_i(t) = (\tau_0/t)^2/\sqrt{1-(\tau_0/t)^2}$ is the response function of different incident angles, and $G_s(t_2-t_1) =< E_s^*(t_1)E_s(t_2) >$ is the temporal-coherence function of the source. Eq.(12) can explain the temporal-coherence gain of the image too. Even if the source field is totally temporal *incoherent* $G_s(t_2-t_1) \propto \delta(t_2-t_1)$, based on Eq.(12) we can find that $G_i(\tau)$ is not a δ-function anymore, so the image is partial temporal coherent. The product of $h_i^*(t_1)h_i(t_2+\tau)$ includes the interference between paths. According to our theory, we calculate the image coherence function $g^{(1)}$ vs time (Fig.11 blue) which agree with our FDTD result (Fig.11 red) pretty well (we will discuss the deviation later).

To further confirm our theory and FDTD results, the *strict* Green's function method [52] is engaged to check our results. *We only include the radiating field (no evanescent wave) in Green's function*. The strict image field vs time is shown in Fig.10c(down), and the image temporal-coherence function $g^{(1)}$ vs time is shown in Fig.11 (blue). In Fig.11, we can see that the FDTD result (red) is almost exactly same as the strict Green's function method (green). But our theory (blue) deviates from the strict result at very large $\tau > 3000\delta_t$ which corresponding to very long path(or very large incident angle). This is understandable since in our theory we neglect the dispersion of NIM totally and only use $v_g(\omega_0)$. For the very-large-angle rays a small index difference (from the dispersion of NIM) can cause large focal-length difference. Hence the deviation is from the focus-filtering effect. When we reduce the FS width of source to an even smaller value (*i.e.* $\Delta\omega_s = \omega_0/500$), the deviation of our theory is smaller.

Although our theory is only a good approximation generally, owing to the picture simplicity and clarity the theory can help us to study more complex systems qualitatively and quantitatively. The *finitely-long* 2D superlens is a good example which is hard to deal by Green's function method. In Fig.(11), we plot the coherent time T_i^{co} vs superlens length L of the FDTD simulation (black) and of our theory (red) , respectively. They coincide with each other pretty well (the deviation reason has been discussed). The increase of the T_i^{co} with the increase of L can be explained simply according our theory. Since the image field is $E_i(t) = \frac{1}{U_0}e^{-i\omega_0 t}\int_{\theta_{min}}^{\theta_{max}} U_s(t-\frac{\tau_0}{cos\theta})d\theta$, the large-angle paths ($\theta > \theta_{max}$ and $\theta < \theta_{min}$)and their contribution to the temporal-coherence gain are missed in the short superlens.

Obviously, Eq.(11) is suitable not only for random quasi-monochromatic source, but also for all quasi-monochromatic fields, such as the slowly-varying Gaussian pulses and slowly switching-on process mentioned by [52]. Our theory can be easily extended to 3D systems too. And owing to the fact that what we find is from the radiating field, so the temporal-coherence gain is not the near-field property. Actually, the new mechanism of the temporal-coherence gain is not limited for the $n \simeq -1$ superlens, also applicable to other superlenses, such as the photonic crystal superlens in [46, 49, 58]. But the specialities of $n \simeq -1$ superlens, such as almost no frequency-filtering (no frequency loss) and no reflection (no energy loss), can be used to design novel optical/photonic coherence-gain devices.

In summary, for the first time we have numerically and theoretically studied the temporal coherence of the superlens image with the quasi-monochromatic source. Numerically, we observe that the temporal coherence of the image can be improved considerably even almost without reflection and filtering effects. Based on new physical picture, we construct a theory to calculate the image field and temporal-coherence function, which excellently agree with the FDTD results and strict Green's function results. The mechanism of the temporal coherence gain is theoretically explained by the different GRT of different paths. Although the evanescent wave is very weak in this study, the coherence of evanescent wave in NIM systems is a very interesting topic which will be discussed elsewhere [66]. Other related topics, such as the spatial coherence which is very essential for the image quality of the superlens, can also be studied through the similar methods. Although our study is within the confinement of classic optics, similar investigation can be extended to the quantum optics [62], and interesting results can be expected. Obviously, the temporal-coherence gain of superlens is another evidence that the NIM phenomena are consistent with the causality [49]. We suppose that the temporal-coherence gain phenomena could be observed in micro-wave experiments[4, 46]. Therefore, this study should have important consequences in the future studies of coherence in NIM systems. The no-reflection and no-frequency-filtering coherence gain of the superlens has some potential applications in the imaging, the coherent optical communication, and the signal processing.

5. The physical picture and the essential elements of the dynamical process for dispersive cloaking structures

Recently, the theory[67, 68] has been developed based on the geometry transformation to realize a cloaking structure (CS), in which objects become invisible from outside. Then a two-dimensional (2D) cylindrical CS[69] and a nonmagnetic optical CS[70, 71] are designed. More surprisingly, the experiment[72] demonstrates that such a 2D CS really works with a "reduced" design made of split-ring resonators. These pioneers' works are really attractive and open a new window to realize the invisibility of human dream. However, so far almost all theoretical[67–71, 73–75] studies of the CS are done in the frequency domain and the geometry transformation idea is supposed to work only for a single frequency, so that the effects of the dispersion have not been intensively studied. As pointed out in Ref. [68] and the quantitatively study in our recent work [7], the dispersion is *required* for the cloaking material to avoid the divergent group velocity. For the dispersive CS, new topics, such as the *dynamical process*, can be introduced in. Dynamical study is essential for the cloaking study since without it we can not answer the questions, such as how can the field gets to its stable state?, is there any strong scattering or oscillation in the process?, and how long is the process?, etc. More important, because the real radars generally are pulsive ones, the dynamical process is critical

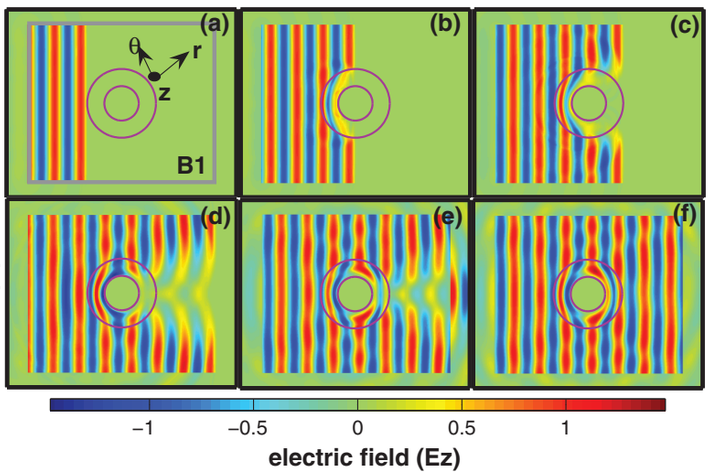

Fig. 13. (Color online) (a) The setup of the system. And the distribution of the electric field at different moments during the process. Parameters are chosen as $A_r = 0.4$, $A_\theta = 1.6$, $A_z = 0.4$ (in the position where $\varepsilon_z < 1$) or $A_z = 1.6$ (where $\varepsilon_z > 1$), and $\gamma = 0.012\omega_0$. (a) $t = 2.28T$. (b) $t = 3.60T$. (c) $t = 4.92T$. (d) $t = 7.20T$. (e) $t = 9.00T$. (f) Stable state. T is the period of the incident EM wave.

for the cloaking effect around the goal frequency. So the dynamical study not only gives us whole physical picture of the cloaking, but also helps us to design more effective cloaks.

In this section, the dynamical process of the electromagnetic (EM) CS is investigated by finite-difference time-domain (FDTD) numerical experiments. In our simulation, the Lorentzian dispersion relations are introduced into the permittivity and the permeability models, then the *real* dynamical process can be simulated[76–78]. Based on numerical simulation, we can follow the details of the dynamical process, such as the time-dependent scattered field, the building-up process of the cloaking effect, and the final stable cloaking state. By tuning the dispersion parameters and observing their effects on the dynamical process and the scattered field, we can find the essential elements which dominate the process. Theoretical analysis of these essential elements can help us to have a deeper physical picture beyond the phenomena and to design more effective cloaks.

The *setup* of the system is shown in Fig. 13(a), similar as the one in Ref. [69]. R_1 and $R_2 = 2R_1$ are the inner and the outer cylindrical radii of the CS, respectively. A perfect electric conductor (PEC) shell is pressed against the inner surface of the CS. The CS is surrounded by the free space with $\varepsilon_0 = \mu_0 = 1$. From the left side, an incident plane wave with working frequency ω_0 is scattered by the CS, the total field and the scattered field can be recorded inside and outside $B1$ respectively by the numerical technique[79]. So the scattering cross-section σ can be calculated easily. Our study is focused on the E-polarized modes, for which only the permittivity and the permeability components ε_z, μ_r, and μ_θ are needed to be considered (For H-polarized modes, considering the corresponding components μ_z, ε_r, and ε_θ, we can obtain the same numerical results in the dynamical process.). All of them are supposed to have the form $1 + F_j(r) \times f_j(\omega)$, where subscript j could be z, r, and θ for ε_z, μ_r, and μ_θ, respectively. The filling factors $F_j(r)$ are only r-dependent, ω_p is the plasma frequency which set to be a constant $\omega_p = 10\omega_0$, and $f_j(\omega) = \omega_p^2/(\omega_{aj}^2 - \omega^2 - i\omega\gamma)$ are the Lorentzian dispersive functions, where

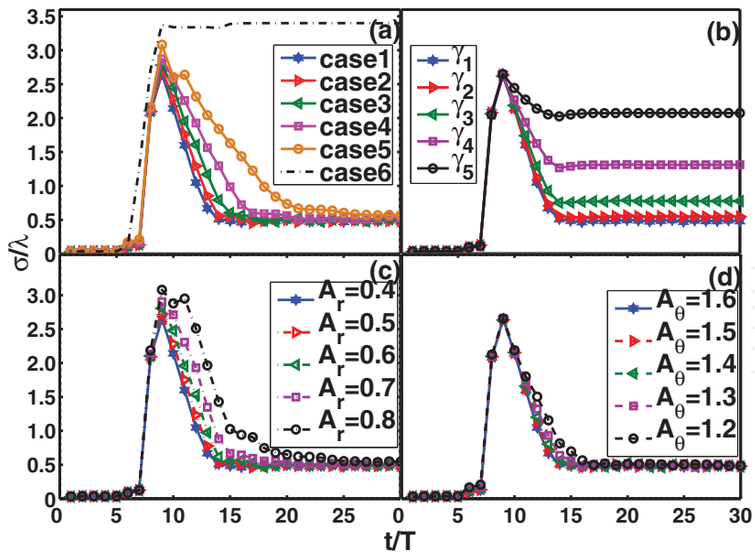

Fig. 14. (Color online) The σ vs t curves. From (a) to (d), $A_z = 0.4$ where $\varepsilon_z < 1$ or $A_z = 1.6$ where $\varepsilon_z > 1$. (a) Keep $\gamma = 0.012\omega_0$ unchanging, choose A_r and A_θ as case 1: $A_r = 0.4$, $A_\theta = 1.6$, case 2: $A_r = 0.5$, $A_\theta = 1.5$, case 3: $A_r = 0.6$, $A_\theta = 1.4$, case 4: $A_r = 0.7$, $A_\theta = 1.3$, case 5: $A_r = 0.8$, $A_\theta = 1.2$. Case 6: only PEC shell without CS. (b) Keep $A_r = 0.4$, $A_\theta = 1.6$ unchanging, choose $\gamma_1 = 0.012\omega_0$, $\gamma_2 = 0.024\omega_0$, $\gamma_3 = 0.048\omega_0$, $\gamma_4 = 0.096\omega_0$ and $\gamma_5 = 0.192\omega_0$. (c) Keep $A_\theta = 1.6$ and $\gamma = 0.012\omega_0$ unvaried, and change A_r. (d) Keep $A_r = 0.4$ and $\gamma = 0.012\omega_0$ unvaried, and change A_θ.

γ is the "resonance width" or called as "dissipation factor," ω_{aj} are the resonant frequency of "atoms" (resonant units) in metamaterials.

For the study of the dispersive CS, we suppose that the real parts of the ε_z, μ_r, and μ_θ always satisfy the geometry transformation of Ref. [69] at ω_0:

$Re[\mu_r(r,\omega_0)] = (r - R_1)/r$, $Re[\mu_\theta(r,\omega_0)] = r/(r - R_1)$, and $Re[\varepsilon_z(r,\omega_0)] = R_2^2(r - R_1)/[(R_2 - R_1)^2 r]$. Then the filling factors $F_j(r)$ at different r can be obtained: $F_r(r) = \{Re[\mu_r(r,\omega_0)] - 1\}/Re[f_r(\omega_0)]$, $F_\theta(r) = \{Re[\mu_\theta(r,\omega_0)] - 1\}/Re[f_\theta(\omega_0)]$, and $F_z(r) = \{Re[\varepsilon_z(r,\omega_0)] - 1\}/Re[f_z(\omega_0)]$.

To investigate the dispersive effect on the dynamical process, we tune the dispersion parameters ω_{aj} in our numerical experiments. We use the working frequency ω_0 as the frequency unit since it is the same for all cases in this section so the ratio $A_j = \omega_{aj}/\omega_0$ represents ω_{aj}. Obviously, for the Lorentzian dispersive relation, the dispersion is stronger when ω_0 and ω_{aj} are closer to each other (the working frequency is near the resonant frequency), or in other words, when A_j approaches *one*. Since there are singular values of real part of ε and μ, in our numerical simulation we have done some approximations,[80] such as we set the maximum and the minimum for ε and μ. Although such approximations will affect the cloaking effect of stable state,[74] we find that the influence of these approximations on the dynamical process is very small and can be neglected.

First, we show an example of evolving electronic field during the dynamical process in Fig. 13 with concrete parameters of A_r, A_θ, A_z, and γ. In Fig. 13(a), the plane wave arrives at the left side of the CS, and is ready to enter the CS. From Fig. 13(b)-13(e), the cloaking effect is

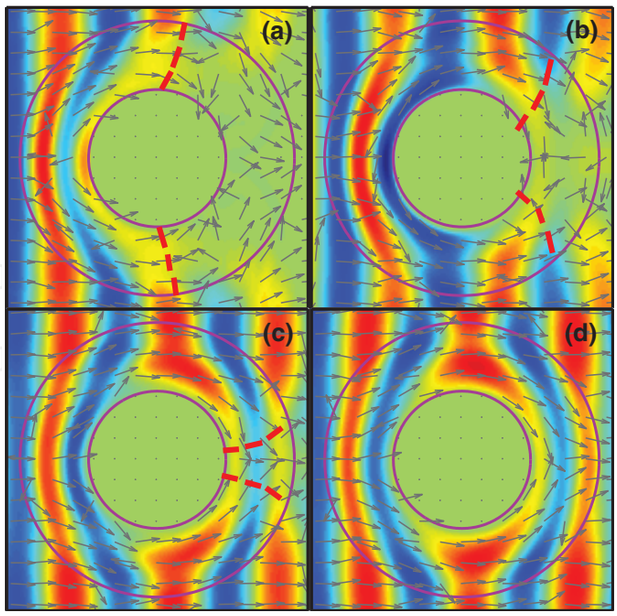

Fig. 15. (Color online) Direction of Poynting vectors and the intensity front (shown by red dashed curves) at moments during the dynamical process. Parameters are chosen as that of Fig. 13. (a) $t = 4.92T$. (b) $t = 7.20T$. (c) $t = 9.00T$. (d) Stable state.

built up step by step, at last, the field gets to the stable state shown in Fig. 13(f). Because of the dispersion, there is an obvious time delay in the cloaking effect and the strong scattered field is observed.

We introduce a time-dependent scattering cross-section $\sigma(t)$ to quantitatively study the dynamical process, which is defined as

$$\sigma(t) = \bar{J}_{scat}(t)/\bar{S}_{inct}, \tag{13}$$

where $t = n \times T$, $n = 0, 1, 2, ...$, T is the period of the incident wave, $\bar{J}_{scat}(t)$ is the one-period-average energy flow of scattered field, and $\bar{S}_{inct}$ is the averaged energy flow density of incident field. To observe the dispersive effect on $\sigma(t)$ during the dynamical process, at the first step, we keep A_z and γ constant and change A_r and A_θ, the results are shown in Fig. 14(a). From the σ versus t curves, we can find the general properties of the dynamical process. First, there is strong scattering in the dynamical process. At the beginning, σ increases rapidly when the wave gets to the CS, then reaches its maximum (at about ninth period). After that, σ starts to decay until it gets to the stable value (of the stable cloaking state). Second, unlike other systems, there is no oscillation in the process. This property will be discussed later. Third, the time length of dynamical process, called as “relaxation time" generally, can be tuned by the dispersion. From Fig. 14(a), we can see that the main dispersive effect is on the decaying process. From case 1 to case 5, A_r and A_θ become closer to *one*, so that the dispersion is stronger. We find that the stronger the dispersion, the longer the relaxation time. For comparing with the cloaking cases, we also show the $\sigma(t)$ of the naked PEC shell in the case 6. From the definition of σ, we know that the area covered by these curve in Fig. 14(a) is proportional to the total scattered energy in the dynamical process. So the CS with *the weaker dispersion will scatter less field* (better cloaking effect) in the dynamical process. But, such

a general conclusion is still not enough for us to get a clear physical picture to understand the cloaking dynamical process.

Next, we check whether the absorption of the CS is important in the process. The absorption is determined by the imaginary part of ε and μ. To study this effect, we hold A_r, A_θ, and A_z constant but modify the dispassion factor γ. We modify the filling factors F_j simultaneously, so that the real parts of ε and μ are kept unchanged at ω_0. In such way, we can keep the dispersion strength almost unchanged, but with the imaginary parts of ε and μ changed. Results in Fig. 14(b) show that the stronger absorption only leads to larger stable value of σ, leaving the relaxation time nearly unchanged. Thus, we can exclude the absorption from the relevant parameter list, since it only influences the $\sigma(t)$ of stable state considerably.

To obtain deeper insight of the dynamical process, we need to study the dynamical process more carefully. From Figs. 13(b)-13(e), we can see that the "field intensity" (shown by different color in the figures) propagates slower inside the CS than that in the outside vacuum. And when the inside field intensity "catches up" the outside one [in Fig. 13(f)], the field in the CS gets to the stable state and the cloaking effect is built up. In fact, this catching-up process of the field intensity can be shown more clearly by the direction of Poynting vectors during the dynamical process. From Figs. 15(a)-15(d), we show the direction of Poynting vectors in moments of Figs. 13(c)-13(f), respectively. In the Fig. 15, we see that there is the "intensity front"(shown by red dashed curve) which separates two regions of the CS. At the right side of the front, the field intensity in the CS is much weaker than the outside and the Poynting vector directions are not regular(especially near the front). But at the left-side region which is swept by the intensity front, the Poynting vectors are very regular and nearly along the "cloaking rays" which was predicted at the coordinate transformation[68]. Since the cloaking effect can be interpreted by the mimic picture that the light runs around the cloaking area through these curved cloaking rays, it is not surprising to find that the stable cloaking state is achieved when the intensity front sweeps through the whole CS and these optical rays are well constructed. The surprising thing is that *the stable cloaking state seems to be constructed locally.* We believe this property is related the original cloaking recipe,[68] which makes the cloaking material is almost impedance matched layer by layer. This also explains why there is no oscillation in the cloaking dynamical process generally. This picture also can interpret the strong scattered field in the dynamical process, since these "irregular rays" at the right-side region of the intensity front must be scattered strongly. Further, we can use this picture to analysis the dynamical process of other incident waves, such as the Gaussian beams, which are composed of different plane-wave components.

With these understanding, now we are ready to find the correlation between the relaxation time and the CS dispersion. It is well known that the field intensity (or energy) propagates at the group velocity V_g, which is controlled by the material dispersion. So the intensity front, which determines the dynamical process, should move in V_g. Thus, we can explain the results in Fig. 14, since our modification of the dispersive parameters can cause the V_g changed. But, because the cloaking material is the strong anisotropic material, the V_g at different directions could be very different. Can we predict more precisely which component dominates the relaxation time? The answer is "yes." In Fig. 15(d), we can see that the stable energy flow in the CS is nearly along the θ direction at most regions of the CS. Then it is reasonable for us to argue that it is the component along the θ direction $V_{g\theta}$, not the component along the r direction V_{gr}, that dominates the relaxation time and the total scattered energy in the dynamical process.

For the anisotropic cloaking material, the $V_{g\theta}$ and V_{gr} can be expressed as: $V_{g\theta} = [\nabla_{\mathbf{k}}\omega(\mathbf{k})]_\theta = (\frac{2c}{\sqrt{\varepsilon_z\mu_r}})/(2 + \frac{\omega}{\varepsilon_z}\frac{d\varepsilon_z}{d\omega} + \frac{\omega}{\mu_r}\frac{d\mu_r}{d\omega})$ and $V_{gr} = [\nabla_{\mathbf{k}}\omega(\mathbf{k})]_r = (\frac{2c}{\sqrt{\varepsilon_z\mu_\theta}})/(2 + \frac{\omega}{\varepsilon_z}\frac{d\varepsilon_z}{d\omega} + \frac{\omega}{\mu_\theta}\frac{d\mu_\theta}{d\omega})$, where c is the velocity of light in vacuum.

In order to illustrate our prediction, the $\sigma(t)$ under different $V_{g\theta}$ and V_{gr} are investigated, respectively. First, we keep the V_{gr} unvaried by holding A_θ, A_z and γ constant [keep $d\varepsilon_z/d\omega$ and $d\mu_\theta/d\omega$ unchanged], only modify A_r to change the $V_{g\theta}$. The results are shown in Fig.14(c), when A_r is closer to *one*, the $V_{g\theta}$ becomes smaller (with larger $d\mu_r/d\omega$), the relaxation time is longer and more energy scattered in the dynamical process. So the larger $V_{g\theta}$ means the better cloaking effect in the dynamical process. On the other hand, when we keep the $V_{g\theta}$ unvaried and change V_{gr} by holding A_r, A_z, and γ constant and modifying A_θ, the results are shown in Fig. 14(d). We find that the relaxation time is almost unchanged with the change of V_{gr}. Obviously, $V_{g\theta}$ is the dominant element in the dynamical process. This conclusion can help us to design a better CS to defend the pulsive radars. In the expression of $V_{g\theta}$, it is also shown how to tune $V_{g\theta}$ by modifying dispersion parameters.

It seems that the larger $V_{g\theta}$, the better cloaking effect in the dynamical process. However, since the V_g (and its components) cannot exceed c generally, there is a minimum limit for the relaxation time of the cloaking dynamical process. We can estimate it through dividing the mean length of the propagation rays by $V_{g\theta}$. In our model, the mean length is $\pi(R_2 + R_1)/2$, about three wavelengths. So the relaxation time can not be shorter than three periods. Figure 14 shows that our estimation is coincident with our simulation results. Actually, here we are facing a very basic conflict to make a “better" CS, which is more discussed in our other works.[7, 81] The conflict is from the fact that the *pretty strong* dispersion is required to realize a good *stable* cloaking effect at a certain frequency,[7, 68] but at this research we show that the *weaker* dispersion can realize a better cloaking effect in the *dynamical* process. At real design of the CS, there should be an optimized trade-off.

Based on causality, the limitation of the electromagnetic cloak with dispersive material is investigated in this section The results show that perfect invisibility can not be achieved because of the dilemma that either the group velocity V_g diverges or a strong absorption is imposed on the cloaking material. It is an intrinsic conflict which originates from the demand of causality. However, the total cross section can really be reduced through the approach of coordinate transformation. A simulation of finite-difference time-domain method is performed to validate our analysis.

6. Limitation of the electromagnetic cloak with dispersive material

Through the ages, people have dreamed to have a magic cloak whose owner can not be seen by others. For this fantastic dream, plenty of work has been done by scientists all over the world. For example, the researchers diminished the scattering or the reflection from objects by absorbing screens[82] and small, non-absorbing, compound ellipsoids[83]. More recently, based on the coordinate transformation, J. B. Pendry, et al theoretically proposed a general recipe for designing an electromagnetic cloak to hide an object from the electromagnetic(EM) wave[68]. An arbitrary object may be hidden because it remains untouched by external radiation. Meanwhile, Ulf Leonhardt described a similar method where the Helmholtz equation is transformed to produce similar effects in the geometric limit[67, 75]. Soon, Steven A. Cummer, et al simulated numerically(COMSOL) the cylindrical version of this cloak structure using ideal and nonideal (but physically realizable) electromagnetic

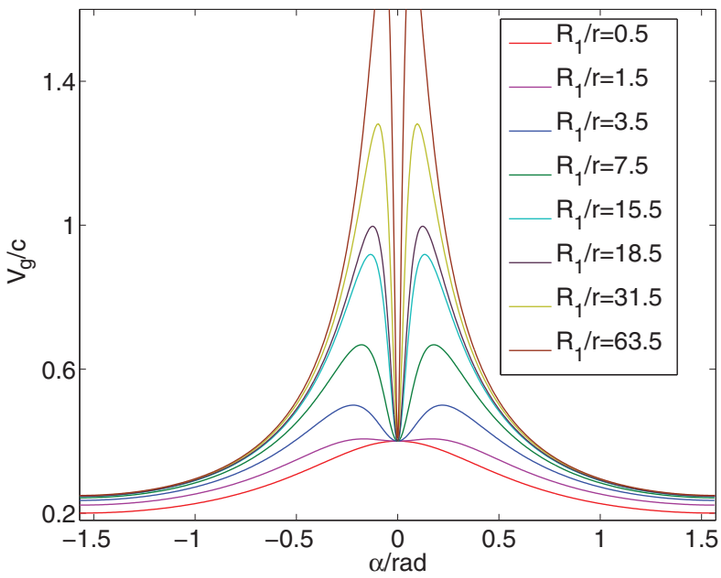

Fig. 16. The group velocity V_g versus α for different R_1/r values

parameters[69]. Especially, Schurig, et al experimentally demonstrated such a cloak by split-ring resonators[72]. In addition, Wenshan Cai , et al proposed an electromagnetic cloak using high-order transformation to create smooth moduli at the outer interface and presented a design of a non-magnetic cloak operating at optical frequencies[70, 71]. According to the general recipe, the electromagnetic cloak is supposed to be perfect or "fully functioned" at certain frequency as long as we can get very close to the ideal design although there is a singularity in the distribution, which has been elucidated further in several literatures [84, 85]. However, in all these pioneering works, the interests are mainly focused on single-frequency EM waves, so that the effects of the dispersion, which is related with very basic physical laws, are not well studied. If the dispersion is introduced into the study, can we have a deeper insight into the cloaking physics?

In this section we will show the ideal cloaking can not be achieved because of another more basic physical limitation—the causality limitation (based on the same limitation, Chen et al obtained a constraint of the band width that limit the design of an invisibility cloak[86]). Starting from dispersion relation and combining with the demand of causality, we will demonstrate that the ideal cloaking will lead to the dilemma that either the group velocity V_g diverges or a strong absorption is imposed on the cloaking material. Our derivation and numerical experiments based on the finite-difference-time-domain(FDTD) methods will show that the absorption cross section will be pretty large and dominate the total cross section for a dispersive cloak, even with very small imaginary parts of permittivity and permeability.

Let's consider a more general coordinate transformation on an initial homogeneous medium with $\varepsilon_i = \mu_i$ in r space: $r' = f(r)$, $\theta' = \theta$, $\varphi' = \varphi$, following the approach in Ref. [87] and [89], we get the following radius-dependent, anisotropic relative permittivity and permeability: $\varepsilon_{r'} = \mu_{r'} = \varepsilon_i(\frac{r}{f(r)})^2\frac{df(r)}{dr}$, $\varepsilon_{\theta'} = \mu_{\theta'} = \varepsilon_i/\frac{df(r)}{dr}$ and $\varepsilon_{\varphi'} = \mu_{\varphi'} = \varepsilon_i/\frac{df(r)}{dr}$. We emphasize that since the transformation is directly acted on the Maxwell equations, the above equations are also suited for the imaginary parts of constitutive parameters, and all physical properties of wave propagation in r space should be inherited in r' space, such as the absorption. This

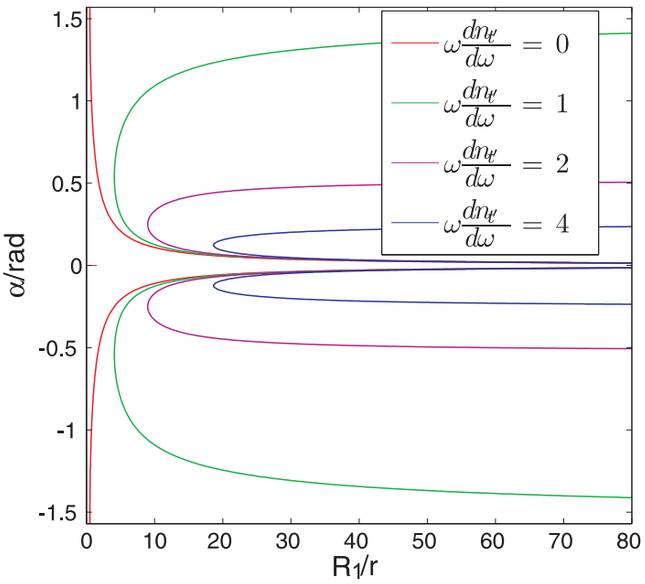

Fig. 17. The relation between R_1/r and α when $V_g = c$ for different $\omega\frac{dn_{t'}}{d\omega}$.

is very important for us to have consistent physical pictures in both spaces. At working frequency ω_0, for a propagating mode with k-vector as $\{k_{r'}, k_{\theta'}, k_{\varphi'}\}$ inside the cloak, we have the dispersion relation of the anisotropic material[87] as: $k_{r'}^2/n_{r'}^2 + k_{t'}^2/n_{t'}^2 = \omega^2/c^2$, where $k_{t'}^2 = k_{\theta'}^2 + k_{\varphi'}^2$, $n_{r'} = \sqrt{\varepsilon_{\varphi'}\mu_{\theta'}} = n_i/\frac{df(r)}{dr}$, $n_{t'} = n_{\theta'} = n_{\varphi'} = \sqrt{\varepsilon_{r'}\mu_{\theta'}} = n_i r/f(r)$, and $n_i = \sqrt{\varepsilon_i\mu_i}$. Then we can define $k_{r'} = \frac{\omega}{c}n_{r'}cos\alpha$ and $k_{t'} = \frac{\omega}{c}n_{t'}sin\alpha$, the group velocity can be obtained as:

$$V_g = c\sqrt{\frac{(cos\alpha)^2}{n_{r'}^2} + \frac{(sin\alpha)^2}{n_{t'}^2}}/((cos\alpha)^2\frac{m_{r'}}{n_{r'}} + (sin\alpha)^2\frac{m_{t'}}{n_{t'}}) \tag{14}$$

Where $m_{r'} = n_{r'} + \omega\frac{dn_{r'}}{d\omega}$ and $m_{t'} = n_{t'} + \omega\frac{dn_{t'}}{d\omega}$.

If the transformation has the following characteristic: $f(r=0) = R_1$, $f(r=R_2) = R_2$, then when $r' \to R_1$ (or $r \to 0$), $n_{t'}$ will tend to zero, and the group velocity is approximated as:

$$V_g \approx \frac{c}{|sin\alpha|\omega\frac{dn_{t'}}{d\omega}} \tag{15}$$

We will discuss Eq.15 in two cases. The first case is with the finite $\frac{dn_{t'}}{d\omega}$. Obviously, V_g will diverge when $sin\alpha \to 0$ for any finite $\frac{dn_{t'}}{d\omega}$. Such divergence is shown in figure 16 for a concrete example, in which the transformation is $r' = f(r) = (R_2 - R_1)r/R_2 + R_1$ as Ref. [68], $R_2 = 2R_1$, thus $n_{r'} = 2$ and $n_{t'} = 2 - 4/(r/R_1 + 2)$. The dispersion parameters are set as $m_{r'} = 2.5$, $\omega\frac{dn_{t'}}{d\omega} = 4$ at working frequency. In figure 16, the curves of V_g vs α are plotted for different R_1/r values. We can see that, for large $R_1/r(r \to 0)$, the group velocity (more precisely, the tangential component of V_g) will diverge at both peaks around $\alpha = 0$.

Because of the causality limitation, it is well-known that the group velocity can not exceed c except in the “strong dispersion" frequency range (or called “resonant range"). But, if the working frequency is in the “strong-dispersion" range of the cloaking material, the absorption must be very strong and it will destroy the ideal cloaking obviously. So perfect invisibility can not be achieved for the finite $\frac{dn_{t'}}{d\omega}$ because it will lead to superluminal velocity or strong absorption.

In addition, the curves with the criterion condition $V_g = c$ on the plane $[R_1/r, \alpha]$ are plotted for different $\omega\frac{dn_{t'}}{d\omega}$ in figure 17. The region to the left of curves is corresponding to $V_g < c$ and the region to the right is corresponding to $V_g > c$. There exists a maximum $max\{R_1/r\}$ for each curve in order that $V_g \leq c$ can be hold for all the α. Especially, for the no-dispersion case $\omega\frac{dn_{t'}}{d\omega} = 0$, we can see that $V_g > c$ at all R_1/r for large α values, which means the whole cloak is not physical if there is no dispersion. This “dispersion-is-required” conclusion can be generally derived from Eq.14, and it is consistent with the analysis in Ref. [68]. From figure 17, we know that the larger $\omega\frac{dn_{t'}}{d\omega}$, the larger $max\{R_1/r\}$. But anyway, for arbitrary finite $\omega\frac{dn_{t'}}{d\omega}$, $max\{R_1/r\}$ can not be infinite, so that the superluminal range always exists.

The second case of Eq.15 is with divergent $\frac{dn_{t'}}{d\omega}$. From the previous discussion, we know that if the ideal cloak exists, the cloak must be dispersive and $\frac{dn_{t'}}{d\omega}$ must be divergent when $r \to 0$. Actually, when $r \to 0$, since $\sqrt{\varepsilon_{r'}} \propto r$, $\frac{dn_{t'}}{d\omega} \propto \frac{d\varepsilon_{r'}}{d\omega}/\sqrt{\varepsilon_{r'}}$ is really divergent for non-zero $\frac{d\varepsilon_{r'}}{d\omega}$. From Eq.15, we can see that now the $V_g \to 0$ for a finite $\frac{d\varepsilon_{r'}}{d\omega}$ (generally true) at all α values except $\alpha = 0$(or π), so that the group velocity difficulty seems to be overcome. But, since the causality limitation, the non-zero $\frac{d\varepsilon_{r'}}{d\omega}$ means non-zero imaginary part of permittivity (non-zero dissipation). The non-zero dissipation and the almost-zero group velocity will result in very strong absorption. This means that the energy of rays near the inner cloaking radius R_1 is almost totally absorbed by the cloaking material. As we pointed out at the beginning that the absorption in r' space should also appear in r space, because of the consistence between two spaces. The strong absorption in r space can be interpreted in the following way. From the transformation (which is also suited for imaginary part), we can find that when $r \to 0$, the finite imaginary part in r' space corresponds to the infinite imaginary part in r space, which also means very strong absorption in the initial homogeneous medium. So the perfect cloaking is still impossible because of the strong absorption which is enforced by the causality limitation.

For a two-dimensional coordinate transformation: $r' = f(r)$, $\theta' = \theta$, $z' = z$, the same conclusions of the causality limitation can be obtained through the similar analysis, although the coordinate transformation and the singularities are different from the three-dimensional case.

Next, we will discuss the physical meaning of the dilemma that either the group velocity V_g diverges or a strong absorption is imposed on the cloaking material. First, it is an intrinsic conflict which can not be solved by the methods, for example, “the system is imbedded in a medium"[68]. We believe that the ideal cloaking is impossible because of the causality limitation and this conclusion is consistent with the statement of previous studies[89] that the perfect invisibility is unachievable because of the wave nature of light. Second, we have to face the question: “ Why the causality is violated for ideal cloaking which is based on the simple coordinate transformation?". Our answer is that the causality is only guaranteed by

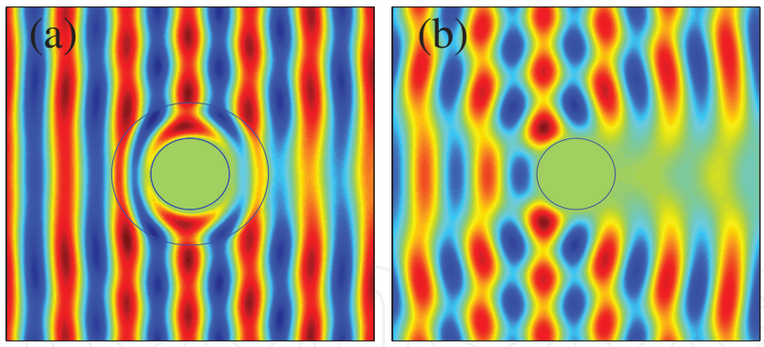

Fig. 18. The snapshots of the electric-field distribution in the vicinity of PEC. (a) the cloaking structure with a PEC at radius R_1, (b) the naked PEC with radius R_1.

the Lorentz co-variant transformation, but the coordinate transformation for ideal cloaking is not Lorentz co-variant. Such violation is obvious if we suppose the initial medium in the r space is not dispersive, such as the vacuum, but as we have pointed out (also mentioned in Ref. [68], the cloaking material (in r' space) must be dispersive to avoid the group velocity over c. Such Lorentz co-variant violation is generally true for ąřtransformation opticsąś since material parameters are non-relativistic, so the causality limitation should be checked widely. Third, from Eq.14, we can find that not only the inner layers of the cloak($r' \to R_1$) but also the other layers($r' > R_1$) must be dispersive. For every layer, a certain dispersive strength is needed to avoid $V_g > c$.

In the following, we will validate that the total cross section can be reduced drastically, and that the perfect cloaking cannot be achieved because of strong absorption by FDTD numerical experiments. Compared with other frequency-domain simulation methods, such as the finite element methods or the transfer-matrix methods, the FDTD simulation can better reflect the real physical process of cloaking. For example, we note that the FDTD calculation will be numerically unstable when the dispersion is not included in the cloak's material. For simplicity, the simulation is limited to two-dimensional cloak[69]. Without lost of generality, only TE modes are investigated in this study (TE modes have the electric field perpendicular to the two-dimensional plane of our model). Thus the constitutive parameters involved here are $\epsilon_{z'}, \mu_{r'}, \mu_{\theta'}$. The dispersion is introduced into our FDTD by standard Lorentz model:

$$\begin{aligned} \tilde{\epsilon}_{z'}(r',\omega)| &= 1 + F_{z'}(r')\omega_{pz'}^2/(\omega_{az'}(r')^2 - \omega^2 - i\omega\gamma_{z'}) \\ \tilde{\mu}_{r'}(r',\omega) &= 1 + F_{r'}(r')\omega_{pr'}^2/(\omega_{ar'}(r')^2 - \omega^2 - i\omega\gamma_{r'}) \\ \tilde{\mu}_{\theta'}(r',\omega) &= 1 + F_{\theta'}(r')\omega_{p\theta'}^2/(\omega_{a\theta'}(r')^2 - \omega^2 - i\omega\gamma_{\theta'}) \end{aligned} \tag{16}$$

$$r' = \frac{R_2(\theta) - R_1(\theta)}{R_2(\theta)} r + R_1(\theta) \tag{17}$$

$$\theta' = \theta \tag{18}$$

Where $\omega_{pz'}, \omega_{pr'}, \omega_{p\theta'}$ are plasma frequencies, $\omega_{az'}, \omega_{ar'}, \omega_{a\theta'}$ are atom resonated frequencies, $\gamma_{z'}$, $\gamma_{r'}$, $\gamma_{\theta'}$ are damping factors and $F_{pz'}$, $F_{pr'}$, $F_{p\theta'}$ are filling factors. In our simulation, an E-polarized time-harmonic uniform plane wave whose wavelength λ_0 in vacuum is $3.75cm$ is incident from left to right. The real parts of the constitutive parameters at $\omega_0 = 2\pi c/\lambda_0$

satisfy the cloaking coordinate transformation[69, 91], and they are $\mu_{r'} = \frac{r'-R_1}{r'}$, $\mu_{\theta'} = \frac{1}{\mu_{r'}}$, $\varepsilon_{z'} = (\frac{R_2}{R_2-R_1})^2 \frac{r'-R_1}{r'}$, where R_1 is $0.665\lambda_0$, R_2 is $1.33\lambda_0$. And the dispersive parameters are set as follows: if $\varepsilon_{z'} > 1$ then $\omega_{az'} = 1.4\omega_0$, else $\omega_{az'} = 0.6\omega_0$, $\omega_{ar'} = 0.6\omega_0$, $\omega_{a\theta'} = 1.4\omega_0$, $\gamma_{z'} = \gamma_{r'} = \gamma_{\theta'} = \omega_0/100$. $\omega_{pz'} = \omega_{pr'} = \omega_{p\theta'} = 4\omega_0$, $F_{z'}(r) = (\varepsilon_{z'} - 1)\frac{(\omega_{az'}^2-\omega_0^2)^2+\omega_0^2\gamma_{z'}^2}{(\omega_{az'}^2-\omega_0^2)\omega_{pz'}^2}$, $F_{r'}(r) = (\mu_{r'} - 1)\frac{(\omega_{ar'}^2-\omega_0^2)^2+\omega_0^2\gamma_{r'}^2}{(\omega_{ar'}^2-\omega_0^2)\omega_{pr'}^2}$, $F_{\theta'}(r) = (\mu_{\theta'} - 1)\frac{(\omega_{a\theta'}^2-\omega_0^2)^2+\omega_0^2\gamma_{\theta'}^2}{(\omega_{a\theta'}^2-\omega_0^2)\omega_{p\theta'}^2}$. In fact, these parameters have many possible choices. The different groups of parameters correspond to different dynamic processes which we will discuss in another section [92].

Figure 18 shows the snapshots of the electric-field distribution in two cases: the cloak with the perfect electric conductor (PEC) at radius R_1(left), and the naked PEC with radius R_1(right). Obviously, the cloak is very effective. Quantitatively, we calculate the absorption cross section and the scattering cross section of the cloak at the stable state, and they are $0.67\lambda_0$ and $0.24\lambda_0$ respectively, while the scattering cross section of the naked PEC is $3.14\lambda_0$. So, with dispersive cloak, the total cross section is three times smaller, and the absorption cross section dominates as we predicted. To emphasize the huge absorption of the cloak, we use a common homogeneous isotropic media, with $\varepsilon = \mu = 1.1$ but all other parameters are the same as the cloak, to replace the cloaking material. Then we find the absorption cross section is only $0.089\lambda_0$ which is about one order smaller. The reason of strong absorption has been discussed before.

Now we can have a full view of cloaking recipe based on the coordinate transformation. First, the cloaking material must be dispersive, and the strong absorption can not be avoided because of the causality limitation. Thus it is not perfectly invisible. Second, the scattering cross section of the dispersive cloak could be small, so that the scattered field is weak. Although the ideal invisibility is impossible, the cloaking recipe still has a main advantage. The “strong-absorption and weak-scattering" property means that the cloak almost can not be observed except from the forward direction. so that such cloak can well defend the ąřpassive radarsąś which detect the perturbation of the original field. It is well-known that at the Rayleigh scattering case, where the radius of the scatterer is much smaller than the wavelength, the absorption cross section could be larger than the scattering cross section because of the diffraction. The cloaking can be thought as giant Rayleigh scattering case, where the light rays are forced to “diffract" around the cloaked area.

In conclusion, the properties of the dispersive cloak are investigated, and the limitation of causality is revealed. Our study shows that the superluminal velocity or a strong absorption can not be overcome since the intrinsic conflict between the coordinate transformation to obtain the cloaking and the causality limitation. In addition, we validate the results using a numerical simulation which is performed in FDTD algorithm with physical parameters. The numerical experiments show that the absorption cross section is dominant and the scattering cross section can be reduced significantly. The study gives us a full view of the cloaking recipe based on the coordinate transformation, and will have further profound influence on the related topics.

7. Summary

In summary, we have investigate the metamaterial systems from group velocity(energy velocity) picture. From these topics, we demonstrate the importance of group velocity in

metamaterial studies. From group velocity, we can find the physical origin of abnormal optical phenomena of metamaterials, such as the “no-transmission no-reflection" on the hyper-medium surface which is from a zero-group-velocity reflecting mode, and the coherence gain of superlens image which is from the different group delay on different paths. From group velocity, we can avoid some traps of violating basic physical limitation, such as the violation of causality limitation in cloaking study. These traps are very serious since the metamaterial from our imagination could exist in this world if violating basic limitations. From group velocity, we can find the key parameter of cloaking dynamical process and help us to optimizing the design of cloak design. From group velocity of evanescent wave, new detecting methods could be found, for example the detecting of QED vacuum polarization by phase change or delay time of evanescent wave. We believe that only with the well-constructed group velocity picture, the deeper understanding of the abnormal optical/photonic properties of metamaterials is possible. All these research works also show that the group velocity study of metamaterials can lead us to many new interesting topics, which are still waiting for further research.

8. Acknowledgement

This work is supported by NKBRPC (Grant No. 2012CB927401), NSFC (Grant Nos. 11004212, 11174309, and 60938004), and the STCSM (Grant Nos. 11ZR1443800 and 11JC1414500).

9. References

[1] V. G. Veselago, Sov. Phys. Usp. 10, 509 (1968).
[2] D. R. Smith, W.J.Padilla, D. C. Vier, S. C. Nemat-Nasser, and S. Schultz, Phys. Rev. Lett. 84, 4184 (2000).
[3] R. A. Shelby, D. R. Smith, S. C. Nemat-Nasser, and S. Schultz, Appl. Phys. Lett. 78, 489 (2001).
[4] R. A. Shelby, D. R. Smith, and S. Schultz, Science 292, 77 (2001).
[5] J. B. Pendry, A. J. Holden, D. J. Robbins, and W. J. Stewart, IEEE Trans. Microwave Theory Tech. 47, 2075 (1999); J. B. Pendry, Phys. Rev. Lett. 85, 3966 (2000).
[6] P. Markos and C. M. Soukoulis, Phys. Rev. B 65, 033401 (2001); Phys. Rev. E 65, 036622 (2002).
[7] P. Yao, Z. Liang, and X. Jiang, Appl. Phys. Lett. 92, 031111 (2008).
[8] Zixian Liang, Peijun Yao, Xiaowei Sun and Xunya Jiang, Appl. Phys. Lett. 92, 131118 (2008)
[9] Zheng Liu, Zixian Liang, Xunya Jiang, Xinhua Hu, Xin Li, and Jian Zi, Appl.Phys. Lett. 96, 113507 (2010)
[10] Brillouin, *Wave Propagation and Group Velocity*, New York:Academic Press Inc., (1960)
[11] J. H. Page, Ping Sheng, H. P. Schriemer, I.Jones, Xiaodun Jing and D. A. Weitzt,Science, 271 634 1996
[12] Hailu Luo, Wei Hu and Zhongzhou Ren, Europhys. Lett. 74 1081(2006).
[13] R.A. Shelby, D.R. Smith, and S. Schultz, Science 92, 792(2001); D.R. Smith and D. Schurig, Phys. Rev. Lett. 90,077405 (2003);C.G. Parazzoli, R.B. Greegor, K. Li, B.E.C. Koltenbah, and M. Tanielian, Phys. Rev. Lett. 90, 107401 (2003).
[14] J. B. Pendry, Phys. Rev. Lett. 85, 3966(2000); N. Fang, H. Lee, C. Sun, X. Zhang, Science 308, 534 (2005); T. Taubner, D. Korobkin, Y. Urzhumov, G. Shvets, R.Hillenbrand, Science 313, 1595 (2006)

[15] J. B. Pendry, Opt. Express 11, 755 (2003); Zhaowei Liu, Hyesog Lee, Yi Xiong, Cheng Sun, and Xiang Zhang, Science 315, 1686 (2007); Igor I. Smolyaninov, Yu-Ju Hung, and Christopher C. Davis, Science 315, 1699 (2007).
[16] Z. Jacob, L. V. Alekseyev, E. Narimanov, Opt. Express 14,8247 (2006); A. Salandrino, N. Engheta, Phys. Rev. B 74, 075103 (2006); Zubin Jacob, Leonid V. Alekseyev, and Evgenii Narimanov, J. Opt. Soc. Am. A 24,A52 (2007); J. B. Pendry, S. A. Ramakrishna, J. Phys. Condens. Matter 14,8463(2002).
[17] Xin Li,Zixian Liang,Xiaohan Liu,Xunya Jiang, and Jian Zi, Appl. Phys. Lett. 93, 171111 (2008).
[18] Hailu Luo, Wei Hu and Zhongzhou Ren, Europhys. Lett. 74 1081(2006).
[19] P. W. Milonni, *Fast Light, Slow Light and Left-Handed Light* Institute of Physics, Great Britain, CRC Press, 2004
[20] As for the explanation of the static solution of the HI it'll be given in another paper.
[21] David R. Smith and Norman Kroll, Phys. Rev. Lett. 85, 2933(2000).
[22] V. A. Podolskiy, and E. E. Narimanov, Phys. Rev. B 71, 201101 (2005); R. Wangberg, J. Elser, E. E. Narimanov, and V. A. Podolskiy, J. Opt. Soc. Am. B. 23, 498 (2006); A. A. Govyadinov, V. A. Podolskiy, Phys. Rev. B 73,115108(2006).
[23] A. Taflove, *Computational Electrodynamics: The Finite-Difference Time- Domain Method* (Artech House, Boston, 1995).
[24] Alessandro Salandrino and Nader Engheta, Phys. Rev. B 74,115108(2006).
[25] N. Fang, H. Lee, C. Sun, and X. Zhang, Science 308, 534 (2005).
[26] Jie Yao,Zhaowei Liu,Yongmin Liu, Yuan Wang,Cheng Sun,Guy Bartal, Angelica M. Stacy and Xiang Zhang, Science 321, 930 (2008).
[27] J. B. Pendry and A. J. Holden and W. J. Stewart, Phys. Rev. Lett. 76, 4773(1996).
[28] A. N. Grigorenko, A. K. Geim, H. F. Gleeson,*et al*, Nature, 438 335(2005)
[29] G. Dolling, M. Wegener, C. M. Soukoulis, and S. Linden, Opt. Lett. 32, 53 (2007).
[30] D. Perkins, Introduction to high energy physics, 4th edition (Cambridge university press, Cambridge, 2000).
[31] N. Ashcroft, N. Mermin, Solid State Physics (Harcourt College Publishers, New York, 1976) ; H. Bruus and K. Flensberg, Many-body quantum theory in condensed matter physics (Oxford university press, Oxford, 2004).
[32] J. Goodman, Statistical Optics (John Wiley & Sons, Inc., New York, 1985).
[33] R. Feynman, QED: the strange theory of light and matter (Princeton university press, Princeton, 1985).
[34] R. Ruffini, G. Vereshchagin and S. Xue, Phys. Rep. 487, 1 (2010).
[35] Y. Ding, A. Kaplan, Phys. Rev. Lett. 63, 2725 (1989).
[36] B. King, A. Piazza and C. Keitel, Nat. photon. 4, 92 (2010).
[37] H. Gies, Phys. Rev. D 61, 085021 (2000).
[38] J. S Heyl and L. Hernquist, J. Phys. A: Math. Gen. 30, 6485 (1997).
[39] R. G. Hunsperger, Integrated Optics: Theory and Technology (Springer-Verlag, New York, 1985).
[40] B.Barwick, D.Flannigan, and A.H. Zewail, Nature 462, 902 (2009).
[41] C. Carniglia and L. Mandel, J. Opt. Soc. Am. 61, 1035 (1971).
[42] J. Kong, Electromagnetic Wave Theory, Electromagnetic Wave Theory (Wiley-Interscience, New York, 1990).
[43] J. Lawall and E. Kessler , Rev. Sci. Instrum. 71, 2669 (2000).

[44] M. Bass, Handbook of Optics, Vol. II (McGraw-Hill, Inc., New York, 1995); W. Su, J. Li and N. Xu, J. Biotechnol. 105, 165 (2003).
[45] T. Tajima, Eur. Phys. J. D 55, 519 (2009).
[46] E. Cubukcu, K. Aydin, E. Ozbay, S. Foteinopoulou, and C. M. Soukoulis Phys. Rev.Lett. 91, 207401 (2003); E. Cubukcu, K. Aydin, E. Ozbay, S. Foteinopoulou, and C.M. Soukoulis, Nature (London) 423, 604 (2003).
[47] J. B. Pendry, Phys. Rev. Lett. 91, 099701 (2003);D. R. Smith, D. Schurig, M. Rosenbluth, S. Schultz, S. A. Ramakrishna, and J. B. Pendry, Appl. Phys. Lett. 82, 1506 (2003).
[48] G. Gomez-Santos, Phys. Rev. Lett. 90, 077401 (2003).
[49] S. Foteinopoulou, E. N. Economou, and C. M. Soukoulis, Phys. Rev. Lett. 90, 107402 (2003); J. B. Pendry and D. R. Smith, Phys. Rev. Lett. 90, 029703 (2003).
[50] X. S. Rao and C. K. Ong, Phys. Rev. B 68, 113103 (2003); X. S. Rao and C. K. Ong, Phys. Rev. E 68, 067601 (2003).
[51] Michael W. Feise, Yuri S. Kivshar, Phys. Lett. A 334 326 (2005)
[52] Lei Zhou, C. T. Chan, Appl. Phys. Lett. 86, 101104 (2005), Y. Zhang, T. M. Grzegorczyk and J. A. Kong, PIER 35,271, (2002)
[53] L. Chen, S. He and L. Shen, Phys. Rev. Lett. 92, 107404(2004).
[54] R. W. Ziolkowski and E. Heyman, Phys. Rev. E 64, 056625 (2001).
[55] S. A. Cummer, Appl. Phys. Lett. 82, 1503 (2003).
[56] P. F. Loschialpo, D. L. Smith, D. W. Forester, F. J. Rachford, and J. Schelleng, Phys. Rev. E 67, 025602(R) (2003).
[57] R. Merlin, Appl. Phys. Lett. 84, 1290 (2004).
[58] C. Luo, S. G. Johnson, J. D. Joannopoulos, and J. B. Pendry Phys. Rev. B 68, 045115 (2003)
[59] Nader Engheta, IEEE Antennas and Wireless Propagation Lett. 1, 10, 2002
[60] Ilya V. Shadrivov, Andrey A. Sukhorukov, and Yuri S. Kivshar, Phys. Rev. E 67, 057602 (2003); A. C. Peacock and N. G. R. Broderick, 11, 2502 (2003).
[61] B. E. A. Saleh, M. C. Teich, *Fundamentals of Photonics* (John Wiley & Sons, New York, 1991)
[62] L. Mandel and E. Wolf *Optical Coherence and Quantum Optics* (Cambridge University, Cambridge, 1995); Marlan O. Scully and M. Suhail Zubairy *Quantum Optics*, (Cambridge University, Cambridge, 1997)
[63] X. Jiang and C. M. Soukoulis, Phys. Rev. Lett. 85, 70 (2000)
[64] In our source frequency range, the index range is about $-1 - i0.0029 \pm (0.006 + i10^{-6})$, so the focal length defference and reflection are very small.
[65] The "group velocity" is not a well-defined value if the working frequency ω_0 is near the resonant frequency ω_a of the NIM. But the GRT is still well-defined.
[66] Xunya Jiang *et. al.* unpublished.
[67] U. Leonhardt, Science 312, 1777 (2006).
[68] J. B. Pendry, D. Schurig, and D. R. Smith, Science 312, 1780 (2006).
[69] S. A. Cummer, B.-I Popa, D. Schurig, and David R. Smith, Phys. Rev. E 74, 036621 (2006).
[70] W. Cai, U. K. Chettiar, A. V. Kildishev, and V. M. Shalaev, Nat. Photonics 1, 224 (2007).
[71] W. Cai, U. K. Chettiar, A. V. Kildishev, V. M. Shalaev, and G. W. Milton, Appl. Phys. Lett. 91, 111105 (2007).
[72] D. Schurig, J. J. Mock, B. J. Justice, S. A. Cummer, J. B. Pendry, A. F. Starr, and D. R. Smith, Science 314, 977 (2006).
[73] H. Chen, B.-I. Wu, B. Zhang, and J. A. Kong, Phys. Rev. Lett. 99, 063903 (2007).

[74] Z. Ruan, M. Yan, C. W. Neff, and M. Qiu, Phys. Rev. Lett. 99, 113903 (2007).
[75] U. Leonhardt, New J. Phys. 8, 118 (2006).
[76] S. A. Cummer, Appl. Phys. Lett. 82, 2008 (2003).
[77] X. Jiang, W. Han, P. Yao, and W. Li, Appl. Phys. Lett. 89, 221102 (2006).
[78] P. Yao, W. Li, S. Feng, and X. Jiang, Opt. Express 14, 12295 (2006).
[79] A. Taflove and S. C. Hagness, *Computational Electrodynamics: The Finite-Difference Time-Domain Method*, 2nd ed. (Artech House, Boston, 2000).
[80] The approximation of permittivity ε and permeability μ in this section are: $Re[\mu_\theta(r,\omega_0)]_{max} = 20$, $Re[\mu_r(r,\omega_0)]_{min} = 1/20$ and $Re[\varepsilon_z(r,\omega_0)]_{min} = 1/5$. unpublished.
[81] H. Chen, Z. Liang, P. Yao, X. Jiang, H. Ma, and C. T. Chan, Phys. Rev. B 76, 241104 (2007).
[82] R. L. Fante, and M. T. McCormack, IEEE Trans. Antennas Propag. 30, 1443(1968).
[83] M. Kerker, J. Opt. Soc. Am. 65, 376(1975). and D. R. Nature Photonics 1, 224 (2007). Graeme W. Milton, Appl. Phys. Lett. 91, 111105 (2007).
[84] Hongsheng Chen, Bae-Ian Wu, Baile Zhang, and Jin Au Kong, Phys. Rev. Lett. 99, 063903 (2007).
[85] Zhichao Ruan, Min Yan, Curtis W. Neff, and Min Qiu, Phys. Rev. Lett. 99, 113903 (2007).
[86] Huanyang Chen, Xunya Jiang, C. T. Chan, arXiv:0707.1126v2.
[87] D. Schurig, J. B. Pendry, and D. R. Smith, Optics Express 14, 9794(2006).
[88] H. Chen and C. T. Chan, Appl. Phys. Lett. 90, 241105 (2007).
[89] Ulf Leonhardt and Thomas G Philbin, New J. Phys. 8, 247(2006).
[90] J. B. Pendry and D. R. Smith, Phys. Rev. Lett. 90, 029703 (2003).
[91] When $r' \to R_1$, $\mu_{\theta'}$ will tend to infinite. In order that it can be realizable in our numerical simulation, we limit its maximum value to 10^3.
[92] Zixian Liang, Peijun Yao, Xunya Jiang, and Xiaowei Sun, unpublished.
[93] G. W. Milton, M. Briane, and J. R. Willis, New J. Phys. 8, 248 (2006).
[94] A. Greenleaf, Y. Kurylev, M. Lassas, G. Uhlmann, http: //www.arXiv:/0703059[math-ph] (2007).
[95] L. D. Landau and E. M. Lifshitz, Electrodynamics of Continuous Media (Pergamon Press, 1975), ch. 11, pp. 315-321
[96] HY Chen and CT Chan, the brief report for the detail of the causality constraint.
[97] T. Koschny, M. Kafesaki, E. N. Economou and C. M. Soukoulis, Phys. Rev. Lett. 93, 107402 (2004).

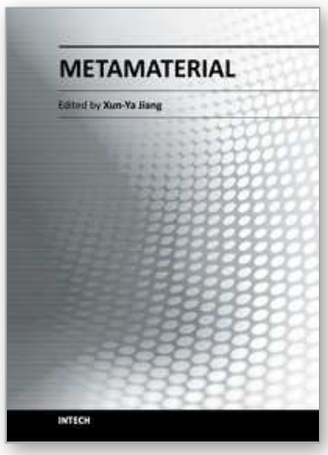

Metamaterial

Edited by Dr. Xun-Ya Jiang

ISBN 978-953-51-0591-6
Hard cover, 620 pages
Publisher InTech
Published online 16, May, 2012
Published in print edition May, 2012

In-depth analysis of the theory, properties and description of the most potential technological applications of metamaterials for the realization of novel devices such as subwavelength lenses, invisibility cloaks, dipole and reflector antennas, high frequency telecommunications, new designs of bandpass filters, absorbers and concentrators of EM waves etc. In order to create a new devices it is necessary to know the main electrodynamical characteristics of metamaterial structures on the basis of which the device is supposed to be created. The electromagnetic wave scattering surfaces built with metamaterials are primarily based on the ability of metamaterials to control the surrounded electromagnetic fields by varying their permeability and permittivity characteristics. The book covers some solutions for microwave wavelength scales as well as exploitation of nanoscale EM wavelength such as visible specter using recent advances of nanotechnology, for instance in the field of nanowires, nanopolymers, carbon nanotubes and graphene. Metamaterial is suitable for scholars from extremely large scientific domain and therefore given to engineers, scientists, graduates and other interested professionals from photonics to nanoscience and from material science to antenna engineering as a comprehensive reference on this artificial materials of tomorrow.

INTECH
open science | open minds

InTech Europe
University Campus STeP Ri
Slavka Krautzeka 83/A
51000 Rijeka, Croatia
Phone: +385 (51) 770 447
Fax: +385 (51) 686 166
www.intechopen.com

InTech China
Unit 405, Office Block, Hotel Equatorial Shanghai
No.65, Yan An Road (West), Shanghai, 200040, China
中国上海市延安西路65号上海国际贵都大饭店办公楼405单元
Phone: +86-21-62489820
Fax: +86-21-62489821

IntechOpen